Discovery of (−)-7-Methyl-2-*exo*-[3′-(6-[^{18}F]fluoropyridin-2-yl)-5′-pyridinyl]-7-azabicyclo[2.2.1]heptane, a Radiolabeled Antagonist for Cerebral Nicotinic Acetylcholine Receptor (α4β2-nAChR) with Optimal Positron Emission Tomography Imaging Properties

Yongjun Gao,[†] Hiroto Kuwabara,[†] Charles E. Spivak,[‡] Yingxian Xiao,[§] Kenneth Kellar,[§] Hayden T. Ravert,[†] Anil Kumar,[†] Mohab Alexander,[†] John Hilton,[†] Dean F. Wong,[†] Robert F. Dannals,[†] and Andrew G. Horti*,[†]

Department of Radiology, Division of Nuclear Medicine, The Johns Hopkins University School of Medicine, 600 North Wolfe Street, Baltimore, Maryland 21287-0816, Cellular Neurophysiology Section, Cellular Neurobiology Branch, IRP, National Institute on Drug Abuse, 333 Cassell Drive, Baltimore, Maryland 21224, and Georgetown University, 3900 Reservoir Road, Washington, D.C. 20007

Received March 27, 2008

Several isomers of 7-methyl-2-*exo*-([^{18}F]fluoropyridinyl-5′-pyridinyl)-7-azabicyclo[2.2.1]heptane have been developed as radioligands with optimized brain kinetics for PET imaging of nAChR. The binding assay demonstrated that all isomers are β-nAChR selective ligands with K_i = 0.02−0.3 nM. The experimental lipophilicity values of all isomers were in the optimal range for the cerebral radioligands (log $D_{7.4}$= 0.67−0.99). The isomers with higher binding affinity manifested slow baboon brain kinetics, whereas the isomer with the lowest binding affinity (K_i = 0.3 nM) ((−)-7-methyl-2-*exo*-[3′-(6-[^{18}F]fluoropyridin-2-yl)-5′-pyridinyl]-7-azabicyclo[2.2.1]heptane, [^{18}F](−)-**6c**) and greatest lipophilicity (log $D_{7.4}$ = 0.99) exhibited optimal brain kinetics. [^{18}F](−)-**6c** manifests a unique combination of the optimally rapid brain kinetics, high BP and brain uptake, and favorable metabolic profile. Pharmacological studies showed that (−)-**6c** is an α4β2-nAChR antagonist with low side effects in mice. This combination of imaging properties suggests that [^{18}F]-(−)-**6c** is a potentially superior replacement for 2-[^{18}F]fluoro-A-85380 and 6-[^{18}F]fluoro-A-85380, the only available nAChR PET radioligands for humans.

Introduction

Cerebral neuronal nAChRs[a] are crucial to normal physiology and have been clearly implicated in various neuropathological processes including Alzheimer's and Parkinson's diseases, Tourette's syndrome, epilepsy, schizophrenia, depression, and tobacco use. A recent review[1] describes many in vivo radioligands that have been developed for the assessment of nAChRs with positron emission tomography (PET) in animals. Two that are derivatives of A-85380, (*S*)-3-(azetidin-2-ylmethoxy)-2-[^{18}F]fluoropyridine **1** (2-[^{18}F]fluoro-A-85380[2]) and (*S*)-5-(azetidin-2-ylmethoxy)-2-[^{18}F]fluoropyridine **2** (6-[^{18}F]fluoro-A-85380[3]) (Figure 1), are now being employed in PET-based evaluations of nAChR in human subjects. Possessing better imaging properties than ^{11}C-nicotine and a lower toxicity than radiolabeled epibatidine analogues, **1** and **2** are satisfactory tools for quantification of thalamic nAChR in the human brain by PET. On the other hand, these two radioligands exhibit the substantial drawbacks of very slow brain kinetics and only moderate BP values.

The slow brain kinetics of **1** and **2** require 6−8 h after injection to reach steady state and, correspondingly, 6−8 h of scanning. Even the bolus + infusion technique that shortens the scanning time does not alleviate the problem of the long postinjection waiting time for human subjects. Consequently, the use of **1** and **2** for human imaging studies is logistically impractical for many PET imaging centers.

The moderate BP values of **1** and **2** make these compounds suitable only for reliable quantification of nAChR located in thalamus, the region with the highest density of the receptor. PET imaging of human brain with **1** and **2** do not demonstrate statistically significant alteration of thalamic nAChR, but they do show altered density of extrathalamic nAChR in Parkinson's disease,[4] smokers,[5] and autosomal dominant nocturnal frontal lobe epilepsy.[6] However, the BP values of the available nAChR radioligands in extrathalamic regions (BP ≤ 0.5) are too low for reliable quantification of the receptor. It is generally accepted that for reliable quantification of a receptor its BP value has to greater than 1.

The objective of this study was to develop a radioligand for PET imaging of the cerebral nAChR having a combination of relatively rapid brain kinetics (requiring a scanning time of less than 120 min), BP^{Th} > 2, and good safety profile. An analysis of previous studies[1] suggests that all azetidine-based nAChR radioligands including **1** and its analogues, regardless of their in vitro properties, manifest slow brain kinetics only if their BP is satisfactorily high and vice versa. Because success in the development of an azetidine-based nAChR radioligand with optimal brain kinetics and high BP value is uncertain, a non-azetidine-based nAChR radioligand was targeted to fulfill the objective of the study.

In the past, several research groups have attempted to develop non-azetidine-based nAChR radioligands with improved brain kinetics.[1,7–11] Recently we reported synthesis and imaging properties of a non-azetidine nAChR radioligand (−)-2-(6′-[^{18}F]fluoro-3,3′-bipyridin-5-yl)-7-methyl-7-azabicyclo[2.2.1]heptane, [^{18}F](−)-**3**[10] (Figure 2). The BP values (Table 4) of this radioligand in thalamus and extrathalamic regions are greater than those of **1**. In addition, radioligand [^{18}F](−)-**3**[10] displays more rapid brain kinetics than our previously developed azetidine-based radioligands (*S*)-5-(azetidin-2-ylmethoxy)-2-

* To whom correspondence should be addressed. Phone: 410-614-5130. Fax: 410-614-0111. E-mail: ahorti1@jhmi.edu.
[†] The Johns Hopkins University School of Medicine.
[‡] National Institute on Drug Abuse.
[§] Georgetown University.

[a] Abbreviations: nAChR, nicotinic acetylcholine receptor; BP, binding potential; Th, thalamus; PET, positron emission tomography.

10.1021/jm800323d CCC: $40.75
Published on Web 07/08/2008

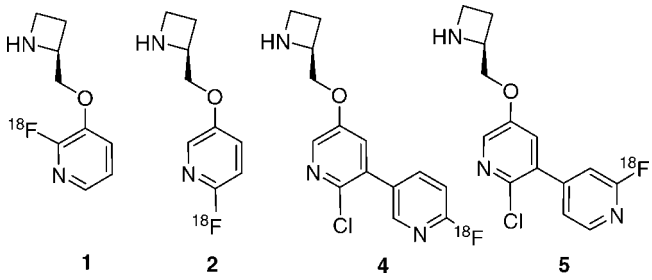

Figure 1. Representative azetidine-based nAChR PET radioligands.

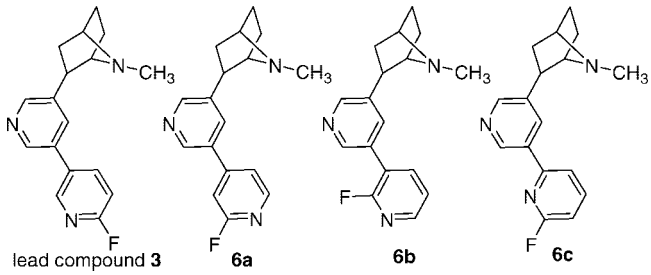

Figure 2. Structures of the lead ligand **3** and novel nAChR ligands **6a**−**c**.

chloro-6′-[^{18}F]fluoro-3,3′-bipyridine **4** ([^{18}F]NIDA52189[1]) and (*S*)-5-(azetidin-2-ylmethoxy)-2-chloro-6′-[^{18}F]fluoro-3,4′-bipyridine **5** ([^{18}F]NIDA522131[1,12]) (Figure 1), which exhibited in the monkey brain equally high BPs as that of [^{18}F](−)-**3**. Despite the improvement in the brain kinetics of [^{18}F](−)-**3**, this compound is only practical for quantification of the cortical regions, and its distribution kinetics are still too slow in thalamus, the region with the highest density of nAChR. Nevertheless, the improvement of the brain kinetics of 7-azabicyclo[2.2.1]heptane derivative [^{18}F](−)-**3** versus the azetidine derivatives **4** and **5** led us to hypothesize that structural analogues of [^{18}F](−)-**3** with slightly reduced binding affinity and comparable lipophilicity might display optimal brain kinetics and good BP values in all brain regions for practical quantitative PET imaging. On the basis of our previous structure−activity relationship work with other series of nAChR ligands,[11] we chose to synthesize isomers of **3** with reduced binding affinity by changing the position of connection of the terminal pyridine ring (para, meta, and ortho) to the internal pyridine ring. In the past, this tactic revealed a series of isomers of nAChR ligands with a wide range of binding affinities.[11] The restraining factor of the current project was the necessity to deal with only 2-fluoropyridine analogues. The 3-fluoropyridine and 4-fluoropyridine derivatives were not targeted because of their potential [^{18}F]-radiolabeling problems and low chemical stability, respectively. As a result, the total number of suitable isomers was four, including the lead compound (−)-**3** (Figure 2). The racemic ligands (±)-7-methyl-2-*exo*-[3′-(2-fluoropyridin-4-yl)-5′-pyridinyl]-7-azabicyclo[2.2.1]heptane (±)-**6a**, (±)-7-methyl-2-*exo*-[3′-(2-fluoropyridin-3-yl)-5′-pyridinyl]-7-azabicyclo[2.2.1]heptane (±)-**6b**, and (±)-7-methyl-2-*exo*-[3′-(6-fluoropyridin-2-yl)-5′-pyridinyl]-7-azabicyclo[2.2.1]heptane (±)-**6c** have been synthesized, and their high affinity enantiomers (−)-7-methyl-2-*exo*-[3′-(2-fluoropyridin-4-yl)-5′-pyridinyl]-7-azabicyclo[2.2.1]-heptane (−)-**6a**, (−)-7-methyl-2-*exo*-[3′-(2-fluoropyridin-3-yl)-5′-pyridinyl]-7-azabicyclo[2.2.1]heptane (−)-**6b**, and (−)-7-methyl-2-*exo*-[3′-(6-[^{18}F]fluoropyridin-2-yl)-5′-pyridinyl]-7-azabicyclo[2.2.1]heptane (−)**6c** have been separated, radiolabeled with positron-emitting isotope ^{18}F, and studied in vitro and in vivo.

One of these isomers, [^{18}F](−)-**6c**, is a high binding affinity $\alpha4\beta2$-nAChR radioligand with unique PET imaging features. In animal studies [^{18}F](−)-**6c** exhibits superior PET imaging properties in comparison with **1** and **2**, including rapid brain kinetics, higher BPs and brain uptake, and a better preliminary safety profile.

Results and Discussion

Chemistry. Synthesis of Fluorinated nAChR Ligands (±)-6a, (±)-6b, and (±)-6c. Stille coupling of 3-bromopyridine derivative **7**[13] with stannane **8**[14] gave 2-bipyridinyl-7-*t*-BOC-7-aza-bicyclo[2.2.1]heptane derivative **10a** (Scheme 1). Suzuki coupling of **7** with pyridylboronic acid **9** yielded **10b**. Another *t*-BOC-protected compound **10c** was prepared by Heck coupling of the norbornene analogue **15**[15] with bromopyridine derivative **14**, obtained by Suzuki coupling of the commercially available pyridines **12** and **13**. Cleavage of *t*-BOC-protective groups of **10a**, **10b**, and **10c** with trifluoroacetic acid yielded secondary amines **11a**, **11b**, and **11c**, respectively. Reductive methylation of **11a**, **11b**, and **11c** with formaldehyde in solution of Na_2HPO_3 afforded the racemic *N*-methyl derivatives **6a**, **6b**, and **6c** in excellent yield.

Synthesis of Brominated Precursors 20a, 20b, and 20c for Radiolabeling of [^{18}F]6a, [^{18}F]6b, and [^{18}F]6c. Racemic bromo derivatives **20a**, **20b**, and **20c** were prepared using the same rationale as that of fluoro analogues **6a**, **6b**, and **6c** (Scheme 2). Stille coupling of iodopyridine derivative **16**[13] with stannane **17**[14] gave *tert*-butoxycarbonyl intermediate **18a**. Deprotection of **18a** with trifluoroacetic acid yielded **19a** in high yield. Suzuki coupling of pyridylboronic acid derivative **12**with halogenated pyridine derivatives **21** or **22** yielded **23** or **24**, respectively. Heck coupling of **23** or **24** with **15** gave *tert*-butoxycarbonyl intermediates **18b** and **18c**, respectively. Treatment of aminopyridines **18b** or **18c** with sodium nitrite in hydrobromic acid in the presence of copper(I) bromide gave bromopyridine derivatives **19b** or **19c**, correspondingly. Reductive methylation of **19a**, **19b**, and **19c** afforded racemates **20a**, **20b**, and **20c**, respectively, in good yield.

The racemic compounds (±)-**6a** and (±)-**6b** and (±)-**20a**−**c** were resolved by chiral semipreparative HPLC to give corresponding enantiomers (Table 1). It is noted that racemate (±)-**6c** could not be fully resolved by chiral semipreparative HPLC under the conditions used here. However, the Boc-protected racemate (±)-**10c** was resolved successfully by chiral semiprep HPLC. Further deprotection of enantiomers of **10c** followed by N-methylation of (+)-**11c** and (−)-**11c** gave the pure (−)-**6c** and (+)-**6c**, respectively (Scheme 3). The chiral analytical HPLC data of (−)-**6c** and (+)-**6c** are shown in Table 1.

In Vitro Studies. In Vitro Binding Affinities of the Novel Ligands. Competition binding assays were performed using two different sources of nAChRs: (1) rat cerebral cortical membranes[16] and (2) seven nAChR subtype cell lines[17] (Table 2). In the binding assays using rat cortex tissue the enantiomers (−)-**6a**−**c** manifested markedly greater (1−2 orders of magnitude) nAChR binding affinities than those of the corresponding (+)-enantiomers (Table 2). This result is in concert with our previous data on (−)-**3** and (+)-**3**.[10] It is noteworthy that the ortho isomer (−)-**6c** manifests lower nAChR binding affinity than do the meta isomers (−)-**3** and (−)-**6b** and para isomer (−)-**6a**. A similar trend (ortho < meta < para) was observed previously in the pyrrolidine series of nAChR ligands.[11]

The competition binding assay results of the defined nAChR subtypes demonstrated that all four isomers (−)-**3**, (−)-**6a**, (−)-**6b**, and (−)-**6c** are $\beta2$-nAChR selective ligands (Table 2). It is

Scheme 1. Synthesis of Fluorinated Racemates **6a**, **6b**, and **6c**[a]

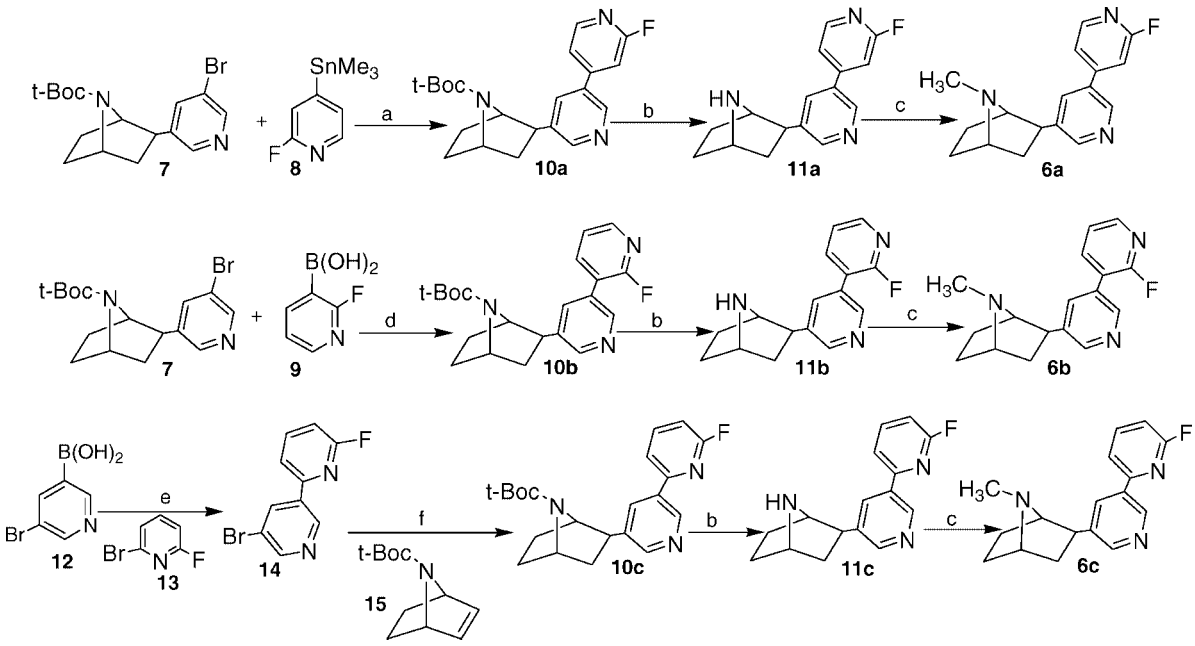

[a] Reagents: (a) $Pd(PPh_3)_4$/toluene; (b) CF_3COOH (TFA); (c) NaH_2PO_3, 37% HCHO; (d) $Pd(PPh_3)_4$, Na_2CO_3, DME; (e) $Pd(PPh_3)_4$, Na_2CO_3, toluene/EtOH/H_2O; (f) $Pd(PPh_3)_4$, piperidine/HCOOH.

Scheme 2. Synthesis of Brominated Racemic Precursors **20a**, **20b**, and **20c**[a]

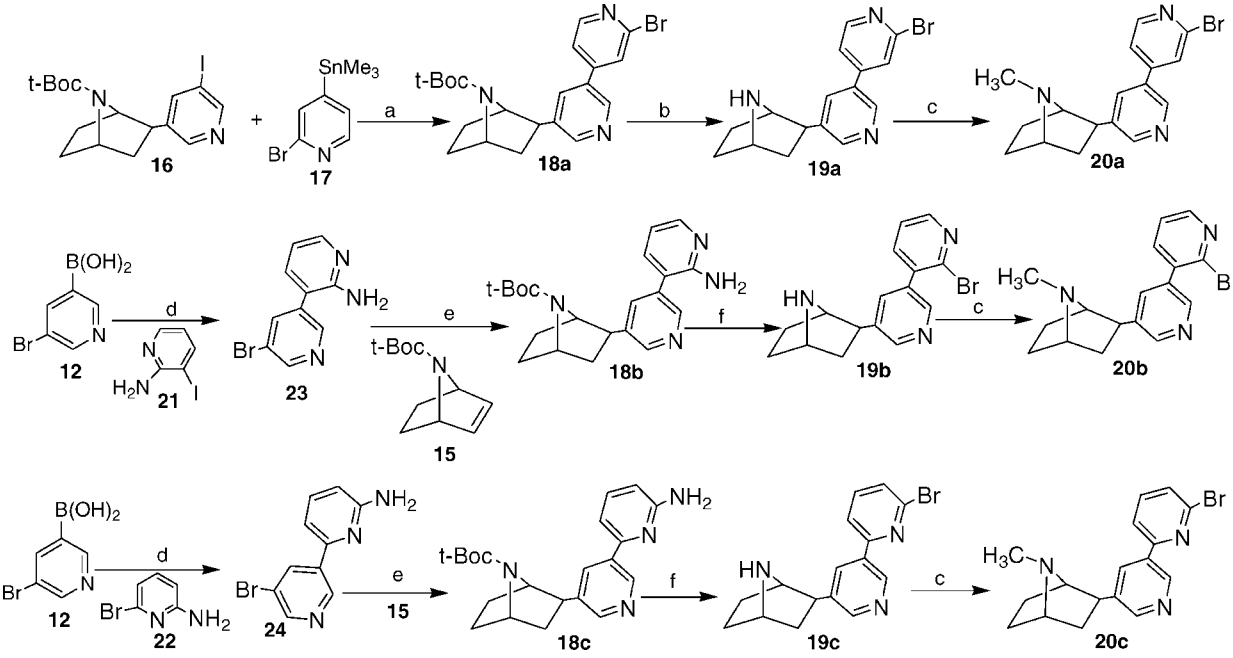

[a] Reagents: (a) $Pd(PPh_3)_4$/toluene; (b) CF_3COOH (TFA); (c) NaH_2PO_3, 37% HCHO; (d) $Pd(PPh_3)_4$, Na_2CO_3, toluene/EtOH/H_2O; (e) $Pd(PPh_3)_4$, piperidine/HCOOH; (f) HBr, CuBr, $NaNO_2$.

interesting that (−)-**6c** showed more than 1000-fold selectivity to α4β2-nAChR, the major subtype in brain, over α3β4-nAChR, the major subtype in peripheral nervous system. These selective binding affinity patterns are dissimilar to that of the non-subtype-selective nAChR ligand epibatidine, but they do resemble that of **1**, a conventional PET ligand for human studies (Table 2). The very high affinities of the isomers (−)-**3**, (−)-**6a**, (−)-**6b**, and (−)-**6c** at α6β2-nAChR subtype are remarkable. Recent results[18] show that striatal α6β2–nAChRs are particularly susceptible to nigrostriatal damage in Parkinson's disease, with a decline in receptor levels that closely parallels losses in striatal dopamine. In contrast, reduction of α4β2-nAChRs is less significant under the same conditions. Therefore, imaging of α6β2-nAChRs is of particular interest for Parkinson's disease.

Determination of Lipophilicity. The experimental lipophilicity values (log $D_{7.4}$ = 0.67−0.99) of **6a**, **6b**, and **6c** were in the optimal range for the central receptor radioligands (log $D_{7.4}$ = 0−3,[1,19] and they are greater than that of **1** (Table 2). The lipophilicity value of **6c** was the highest within the series of the isomers **3**, **6a**, **6b**, and **6c**.

Functional Assay. Whole cell patch clamp experiments with (−)-**6c** were performed using the SH-EP1 cell line that was

Table 1. Enantiomers **6a**, **6b**, **10c**, **20a**, **20b**, and **20c** Resolved by Semipreparative Chiral HPLC (Chiralcel OD Column, 10 mm × 250 mm), Flow Rate = 4 mL/min

enantiomer	HPLC eluent[a]	retention time,min	ee,[b] %	$[\alpha]_D^{22}$ (mg/mL[c])
(−)-**6a**	(A) 50:450:2	10.9	>98	−16.8 (0.78)
(+)-**6a**	(A) 50:450:2	11.9	>98	16.0 (0.83)
(−)-**6b**	(A) 50:450:2	9.7	>98	−16.3 (0.95)
(+)-**6b**	(A) 50:450:2	10.9	>98	17.5(0.97)
(−)-**6c**[d]	(C) 50:950:1	9.1	>98	−9.3 (0.58)
(+)-**6c**[d]	(C) 50:950:1	7.1	>98	7.3 (0.52)
(−)-**10c**	(B) 34:466:2	15.0	>98	−17.3 (0.84)
(+)-**10c**	(B) 34:466:2	16.2	>98	15.8 (0.93)
(−)-**20a**	(A) 50:450:2	13.3	>98	−18.7(0.75)
(+)-**20a**	(A) 50:450:2	14.5	>98	17.2 (0.87)
(−)-**20b**	(A) 50:450:2	11.2	>98	−1.46 (1.53)
(+)-**20b**	(A) 50:450:2	12.6	>97	1.53 (1.43)
(−)-**20c**	(A) 30:470:2	13.1	>98	−9.5(1.19)
(+)-**20c**	(A) 30:470:2	13.9	>95	8.4 (1.27)

[a] HPLC eluent composition: A = 2-propanol/hexane:Et_3N, B = 2-propanol/hexane/Et_2NH, C = ethanol/hexane/Et_2NH. [b] ee = enantiomeric excess. [c] Sample concentration in chloroform. [d] Analytical chiral HPLC, Regis Pak (4.6 mm × 250 mm), 2 mL/min. The preparative amounts of enantiomers (+)-**6c** and (−)-**6c** were obtained via the enantiomers **10c** (Scheme 3).

Scheme 3. Preparation of Enantiomers (+)-**6c** and (−)-**6c**

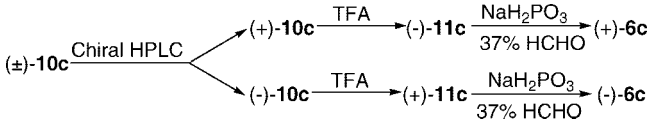

stably transfected with the human α4β2 nicotinic acetylcholine receptor.[20] Figure 3A shows responses to 30 μM acetylcholine (ACh) and 10 nM (−)-**6c** in the same cell. The inset shows that while (−)-**6c** has feeble agonist properties that generate 13 pA of current, these are vanishingly small (<0.3%) in comparison with the 5.3 nA generated by 30 μM ACh. To evaluate the activity of (−)-**6c** for its ability to inhibit ACh activation, each test first established control responses to 30 μM ACh at a given cell. After the control responses stabilized, we superfused (−)-**6c** continuously, retesting the response of 30 μM ACh with (−)-**6c** at about 3.5-min intervals. Figure 3B shows that about 20 min are required to establish equilibrium. The normalized responses at this time are plotted against the (−)-**6c** concentration in Figure 3C, where the weighted data points are fitted to a competitive inhibition function. The fitted K_D value for (−)-**6c** was 0.54 ± 0.08 nM, which concurs with the K_i value given in Table 2.

At the nanomolar concentrations of (−)-**6c** effective in these studies, coapplication of ACh and (−)-**6c** without preincubation showed no blockade. This observation could be a result of (a) the low concentrations of (−)-**6c** combined with a forward (binding) rate constant that may be much lower than that of ACh or (b) the fact that (−)-**6c** acts as a "desensitizer",[21] whereby even high concentrations of the antagonist require minutes to bind to a desensitized state of the receptor. To test the latter possibility, when the high concentration of 1 μM (−)-**6c** was coapplied with 30 μM ACh, the peak amplitudes were reduced to 14 ± 3% of control levels. This immediate blockade supports the view that (−)-**6c** is mainly a competitive antagonist, not a "silent desensitizer".[21]

Radiochemistry. Radiolabeling of [^{18}F](−)-**6a**, [^{18}F](−)-**6b**, and [^{18}F](−)-**6c** (Scheme 4) was performed remotely in one step by 1,10-diaza-4,7,13,16,21,24-hexaoxabicyclo[8.8.8]-hexacosane assisted radiofluorination of the respective bromo precursors (−)-**20a**, (−)-**20b**, and (−)-**20c** using a modified FDG radiochemistry synthesis module (Microlab, GE) followed by the reverse-phase semipreparative HPLC separation. The final products [^{18}F](−)-**6a**, [^{18}F](−)-**6b**, and [^{18}F](−)-**6c** were prepared with high radiochemical yield (16−47% at the end of synthesis, non-decay-corrected), specific radioactivity in the range of 185 GBq to 1.8 TBq (5000−49500 mCi/μmol), and radiochemical purity greater than 98%. The radiosynthesis of [^{18}F](−)-**6a**, [^{18}F](−)-**6b**, and [^{18}F](−)-**6c** is substantially simpler than that of **1** or **2**, and it provides a higher radiochemical yield, excellent specific radioactivity, and radiochemical purity of the final products. Note that the wide range of specific radioactivities of the final products is due, in part, to the difference in the starting doses of [^{18}F]fluoride (0.12−1.4 Ci). Usually, a greater starting dose provides a better specific radioactivity of the final product.[1]

The enantiomeric purity of [^{18}F](−)-**6a**, [^{18}F](−)-**6b**, and [^{18}F](−)-**6c** (>99% ee) was determined by chiral HPLC (Table 1), whereas their identities were confirmed by reverse-phase HPLC coinjection with standard (−)-**6a**, (−)-**6b**, and (−)-**6c**, respectively (see Supporting Information).

In Vivo Studies. PET Imaging in Baboon. Radioligands [^{18}F](−)-**6a**, [^{18}F](−)-**6b**, and [^{18}F](−)-**6c** were studied in baboon PET experiments as potential nAChR-imaging agents. All three radioligands exhibited exceptionally high uptake in the baboon brain (Figures 4 and 5) with regional distribution that was consistent with known distribution of α4β2-nAChR.[22] These imaging properties are in agreement with high nAChR binding affinity and optimal lipophilicity of the radioligands (Table 2).

The radioligand [^{18}F](−)-**6a** manifested relatively slow brain kinetics (Figure 4, left; Table 3) similar to those of the previously studied [^{18}F](−)-**3**.[10] The accumulation of radioactivity of [^{18}F](−)-**6a** in the nAChR-rich thalamus peaked at about 2.5−3 h after injection (Figure 4, left), and it did not reach the steady state within the 3 h of scanning. The slow brain kinetics of [^{18}F](−)-**6a** in thalamus is not a surprise, taking into consideration the very high binding affinity of this radioligand (Table 2). It is well-known that CNS radioligands with very high affinity often display slow brain kinetics[23] due to their slow dissociation rates with receptor.[24] In the frontal cortex, the region with relatively lower density of nAChR, the accumulation of radioactivity of [^{18}F](−)-**6a** peaked at 15−30 min postinjection (Figure 4, left).

The radioligand [^{18}F](−)-**6b** displayed more rapid brain kinetics than [^{18}F](−)-**6a** (Figure 4, Table 3) even though the binding affinity of [^{18}F](−)-**6b** is similar to that of [^{18}F](−)-**6a**. After the injection of [^{18}F](−)-**6b** the uptake of radioactivity in the baboon brain reached its maximum at 65−70 min after injection (Figure 4, right), whereas the clearance half-life from thalamus was about 210 min (Table 3).

The last compound of the series, ortho-isomer [^{18}F](−)-**6c**, having the highest lipophilicity value and lowest binding affinity within the series (Table 2), was the most interesting. In two baboon baseline bolus studies (Figure 5) the kinetics of [^{18}F](−)-**6c** radioactivity distribution was optimally reversible in all brain regions. In the nAChR-rich thalamus the accumulated radioactivity rapidly reached its maximum value (7−28 min, ∼600% standardized uptake value (% SUV)) followed by a robust washout. In the other brain regions with lower density of nAChR, the radioactivity peaked at 5−10 min after administration.

Subcutaneous preadministration of α4β2-nAChR ligand cytisine (Figure 5, left) blocked accumulation of radioactivity induced by injection of [^{18}F](−)-**6c**, thus confirming that in vivo binding of this radioligand in the baboon brain is mediated by α4β2-nAChR.

Table 2. Experimental Lipophilicity (log $D_{7.4}$) and nAChR Inhibition Binding Affinity (K_i) of Epibatidine **1** and Novel Ligands **3**, **6a**, **6b**, and **6c**[a]

			K_i, nM[c,d] (defined rat nAChR subtypes)						
compd	log $D_{7.4}$	K_i, nM[b] (rat cortex)	α4β2	α2β2	α2β4	α3β2	α3β4	α4β4	α6β2
epibatidine		0.045 ± 0.009 (n = 15)	0.061	0.025	0.095	0.035	0.57	0.16	
1	−1.43[14]		1.33	1.44	181	3.02	3680	188	
(−)-**3**	0.46 ± 0.07[10]	0.05[10]	0.011	0.009	0.51	0.093	30	0.31	0.047
(+)-**3**		2.1[10]							
(±)-**6a**	0.74 ± 0.02	0.14; 0.19							
(−)-**6a**		0.11; 0.13	0.019	0.015	0.84	0.13	39	0.58	0.031
(+)-**6a**		1.41; 1.29							
(±)-**6b**	0.67 ± 0.02	0.16							
(−)-**6b**		0.06; 0.05	0.058	0.034	0.66	0.68	41	0.71	0.021
(+)-**6b**		7.35; 7.72							
(−)-**6c**	0.99 ± 0.05	0.31; 0.34	0.26	0.26	7.8	4	310	6.2	0.95
(+)-**6c**		4.67; 6.67							

[a] Measurements of log$D_{7.4}$ and K_i values are briefly described in Experimental Section. [b] The binding assay using rat cerebral cortex tissue was performed commercially by NovaScreen Biosciences (Hanover, MD) under experimental conditions similar to those previously published,[16] using [^{3}H]epibatidine as a radioprobe. [c] The binding affinities of **1** and the ligands **3**, **6a**−**c** to the seven defined heteromeric nAChR subtypes were performed under conditions described previously.[17,38] The K_i values of these ligands to the defined nAChR subtypes shown are the mean of two to three measurements. [d] The K_i values of epibatidine were published previously[17] and are presented here for comparison.

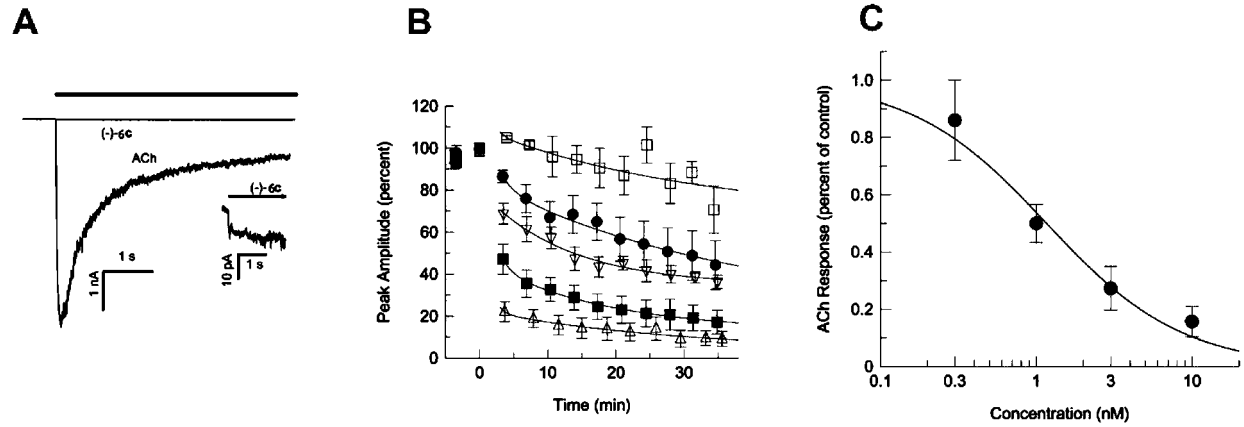

Figure 3. New ligand (−)-**6c** exhibits functional properties of an α4β2-nAChR antagonist at the SH-EP1 cells stably expressing human α4β2 nAChR. Panel A shows that, in comparison with ACh, (−)-**6c** is a vanishingly weak partial agonist (inset). Drug application is denoted by the horizontal bar. Panel B shows normalized mean values and standard errors for tests of 30 μM ACh at various times in the absence ("rundown", open squares) and presence of (−)-**6c** as a function of time. Concentrations of (−)-**6c** are 0.3 nM (filled circles), 1 nM (downward triangles), 3 nM (filled squares), and 10 nM (upward triangles). Panel C shows the inhibition curve (corrected for rundown) fitted to the function for competitive inhibition.

Scheme 4. Radiosynthesis of [^{18}F](−)-**6a**, [^{18}F](−)-**6b**, and [^{18}F](−)-**6c**

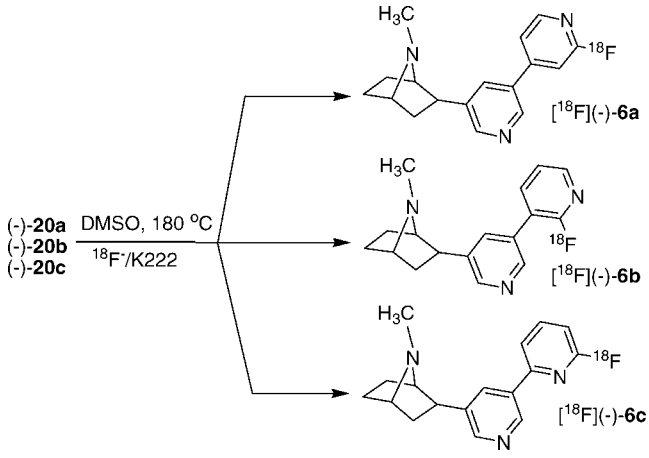

Required Duration of the PET Scanning Time. Estimation of PET outcome variables of [^{18}F](−)-**6a**, [^{18}F](−)-**6b**, and [^{18}F](−)-**6c** in the baboon brain was performed using constrained and nonconstrained k4-models. The PET modeling demonstrated a dependence of the values of the outcome variables versus the scanning time (Figure 6). If the scanning time is too short, the values are inaccurate. A certain scanning time is required to reach constancy in the outcome variables values (Figure 6, Table 3).

The kinetics of [^{18}F](−)-**6a** in the baboon thalamus was so slow that estimates of total volume of distribution (VD) did not reach constancy during the 180 min of scanning time. The estimated value of BP^{Th} for [^{18}F](−)-**6a** (Table 3) is likely to be approximately 20% lower than the maximal value. There was little effect of the scanning time (within 90−180 min) on calculated values of outcome variables of [^{18}F](−)-**6a** for extrathalamic regions (Figure 6, right), and the sufficient scanning time after bolus injection for the accurate quantification of nAChR with [^{18}F](−)-**6a** in the frontal cortex was about 90 min (Figure 6, right).

The brain kinetics of [^{18}F](−)-**6b** in thalamus is faster than that of **1** (Table 3). Thus, only 2−2.5 h of postinjection scanning is necessary for accurate estimation of BP^{Th} of [^{18}F](−)-**6b** versus 6−8 h for **1**. In the cortical regions the required scanning time for [^{18}F](−)-**6b** is even shorter (Figure 6, right, Table 3). These data suggest that [^{18}F](−)-**6b** might be a radiotracer of choice for PET imaging of nAChR in the extrathalamic regions. This radioligand is superior to the previous extrathalamic nAChR radioligands and [^{18}F](−)-**3**,[10] **4**,[14] **5**[12,25] and merits further investigation.

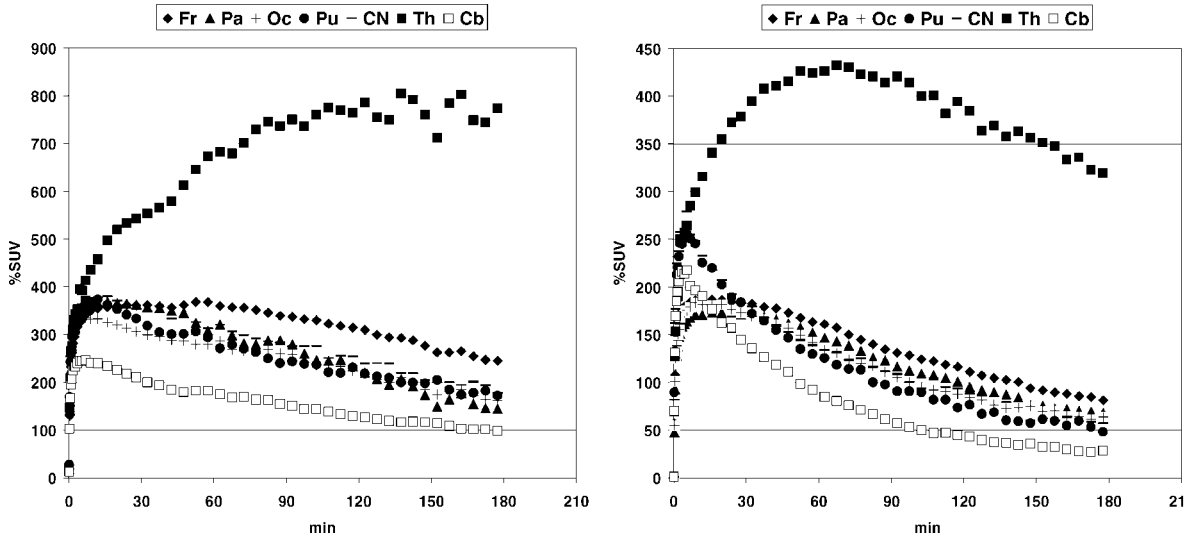

Figure 4. Comparison of the baseline time-uptake curves of [^{18}F]**6a** (left panel) (dose, 6.5 mCi, 43 771 mCi/μmol) and [^{18}F]**6b** (right panel) (dose, 5.5 mCi, 7068 mCi/μmol) in the baboon brain regions. Symbols are as follows: frontal cortex (Fr), parietal cortex (Pa), occipital cortex (Oc), putamen (Pu), caudate nucleus (CN), thalamus (Th), cerebellum (Cb).

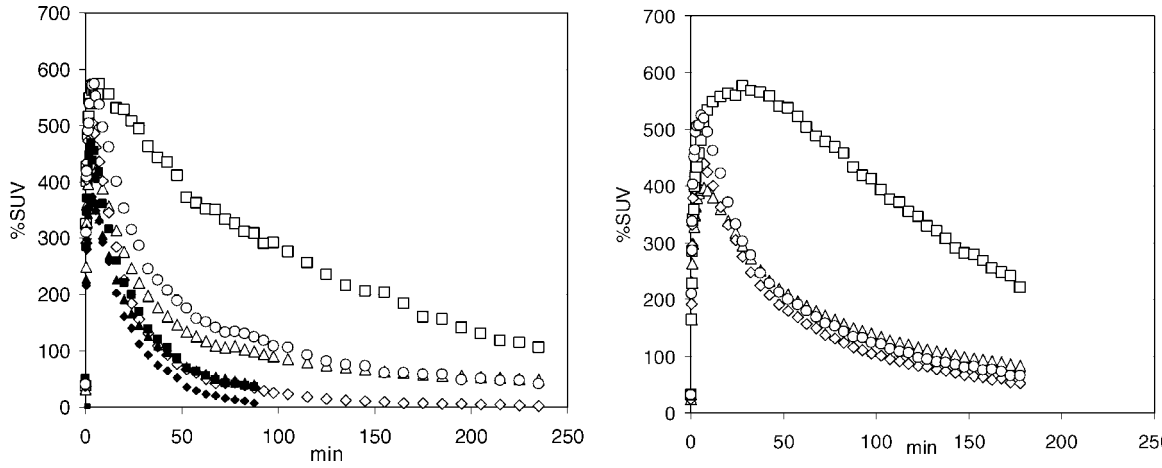

Figure 5. Baseline (open symbols) and blockade with cytisine (2 mg/kg, sc) (filled symbols) time-uptake curves of [^{18}F]**6c** in the brain regions of the baboon no. 15070 (left panel) and the baboon no. 459 (right panel). Symbols are as follows: squares = thalamus; triangles = cortex; circles = basal ganglia; diamonds = cerebellum. Injected doses of [^{18}F]**6c** are as follows: baboon no. 15070 (32.7 kg), baseline, 10.3 mCi, specific radioactivity = 11265 mCi/μmol; blockade, 10.4 mCi, specific radioactivity = 2300 mCi/μmol; baboon no. 459 (25.7 kg), baseline, 12.1 mCi, specific radioactivity = 21 776 mCi/μmol.

Table 3. Comparison of PET Imaging Properties of **1**, [^{18}F](−)-**3**, **5**, and Novel nAChR Ligands [^{18}F](−)-**6a**, [^{18}F](−)-**6b**, [^{18}F](−)-**6c** in Baboon Brain[a]

PET radioligand for imaging of $\alpha4\beta2$-nAChR		peak of uptake in thalamus, min	clearance from thalamus $t_{1/2}$, min	BP	scanning time for accurate quantification of nAChR, h
1	rhesus[43]	80−90	270	2^{Th}	$5-6^{Th}$
	baboon[44]	90−140	nd	2^{Th}	$6-8^{Th}$
	human[45]	>240	nd	2^{Th}	$7-8^{Th}$
5	rhesus[12]	>480	nd	$\sim7^{Th}$, $\sim1^{Ctx}$	$>8^{Th}$, 6^{Ctx}
[^{18}F](−)-**3**	baboon[10]	180	nd	7^{Th}, 1.1^{Ctx}	$>3^{Th}$,[b] 1.5^{Ctx}
[^{18}F](−)-**6a**	baboon	160	nd	7^{Th}, 1.0^{Ctx}	$>3^{Th}$, 1.5^{Ctx}
[^{18}F](−)-**6b**	baboon	65−70	210	7.3^{Th}, 1.3^{Ctx}	$2-2.5^{Th}$, 1^{Ctx}
[^{18}F](−)-**6c**	baboon	7, 28	80, 105	$2.1-4.8^{Th}$, $0.6-1.0^{Ctx}$	1.5^{Th}, 1.5^{Ctx}

[a] Abbreviations: Th = thalamus; Ctx = cortex; nd = not determined due to insufficient scanning time. [b] Determined in this study.

In two baseline studies the BP^{Th} value of [^{18}F](−)-**6c** was higher than that of **1** (Table 3). PET modeling (Figure 6) demonstrated that it required 90−100 min for both the volume of distribution and BP to come within >95% of respective time-invariant estimates in all brain regions in the baboon brain. For comparison, at least 6 h of scanning is needed for PET quantification of **1** (Figure 6, left), the only available nAChR radioligand for humans.

Effect of Anesthesia in Baboon. When developing a radioligand with improved brain kinetics in humans, one should take into consideration the species differences between human and nonhuman primates that are used in the preclinical phase and the effects of anesthesia. There is a known effect of anesthesia in animals on the brain kinetics of **1**, an established nAChR PET radiotracer. The comparison of effects of anesthetics isoflurane (Iso) and ketamine/xylazine (K + X) on the brain

Table 4. HPLC Analysis of Radiolabeled Metabolites of [^{18}F](−)-**6c** in Mouse Blood and Brain (30 min after Injection) and Baboon Blood (60 min after Injection)

	metabolite 1, % (retention time = 1.5 min)	metabolite 2, % (retention time = 6.1 min)	metabolite 3, % (retention time = 6.7 min)	parent, [^{18}F](−)-**6c**, % (retention time = 9 min)
mouse blood	64.6	17.0	6.1	12.3
mouse brain	nondetectable	nondetectable	7.5	92.5
baboon blood	73.2	11.0	0.9	14.9

kinetics of **1** in baboon demonstrated that the brain kinetics are slightly faster with K + X.[26] However, despite the influence of anesthesia on the brain distribution of **1** in monkey and baboon, the scanning time required for accurate estimation of BP in these species (5−7 h) is similar to the scanning time in human subjects (6−7 h). This observation suggests that the brain kinetics of **1** in anesthetized nonhuman primates and nonanesthetized human subjects are similar.

One of the main reasons that anesthetic agents "accelerate" the brain kinetics is an increase of the peripheral metabolism and blood flow. For baboon studies with the anesthetic propofol, we used an infusion rate of 0.3−0.4 (mg/kg)/h. The effects of propofol on metabolism and blood flow have been studied in the past.[27] That study demonstrated that propofol does not display any significant effect on cerebral blood flow and metabolism in baboon at the infusion rate up to 3 (mg/kg)/h. At very high infusion rates (6 and 12 (mg/kg)/h) propofol decreased the cerebral blood flow (28% and 36%, respectively) and cerebral metabolic rates of oxygen (5% and 22%) and glucose (18% and 36%). The infusion rate of propofol that we employ for baboon PET studies (0.3−0.4 (mg/kg)/h) is substantially lower. Therefore, it is likely that the anesthetic agent propofol does not have a significant effect on the brain kinetics of the radioligands studied here, and the future translational assessment (baboon-to-human) of the radioligand [^{18}F](−)-**6c** should be straightforward.

Metabolism of [^{18}F](−)-6c in Mice and Baboon. Metabolites of [^{18}F](−)-**6c** in mice and baboon were studied by HPLC using a general column-switching procedure described elsewhere.[28] Analysis of blood samples from the animals showed that [^{18}F](−)-**6c** undergoes metabolism in both species with generation of three hydrophilic metabolites (Table 4). No lipophilic metabolites of [^{18}F](−)-**6c** have been observed in the two species of animals. The total percentage of metabolites in the blood increased in the course of the studies reaching a gently sloping plateau (85−90%) in 30 and 60 min after injection in mice and baboon, respectively (data not presented). HPLC analysis of the mouse brain extract demonstrated that only a small amount (7.5%) of metabolite 3 (Table 4) penetrates the mouse brain when the metabolic conversion of the parent compound reaches the plateau in the blood. The relative amount of this metabolite in the baboon blood is about 6-fold lower than that in the mouse blood. Therefore, we hypothesized that the presence of the radiolabeled metabolite of [^{18}F](−)-**6c** in the baboon brain is insignificant (<2%) and can be ignored in the PET modeling.

In Vivo Studies with [^{18}F](−)-6c in Mice. Because [^{18}F](−)-**6c** appeared to be the best radiotracer for further studies in humans, we performed preliminary pharmacological and toxicological evaluation of this radioligand in mice. The brain regional distribution studies of [^{18}F](−)-**6c** (Figure 7) and saturation of its binding with "cold" (−)-**6c** (Figure 8) were performed using a previously described dissection/counting procedure.[29]

After intravenous injection of [^{18}F](−)-**6c** a high accumulation of radioactivity was observed in the mouse brain. The peak

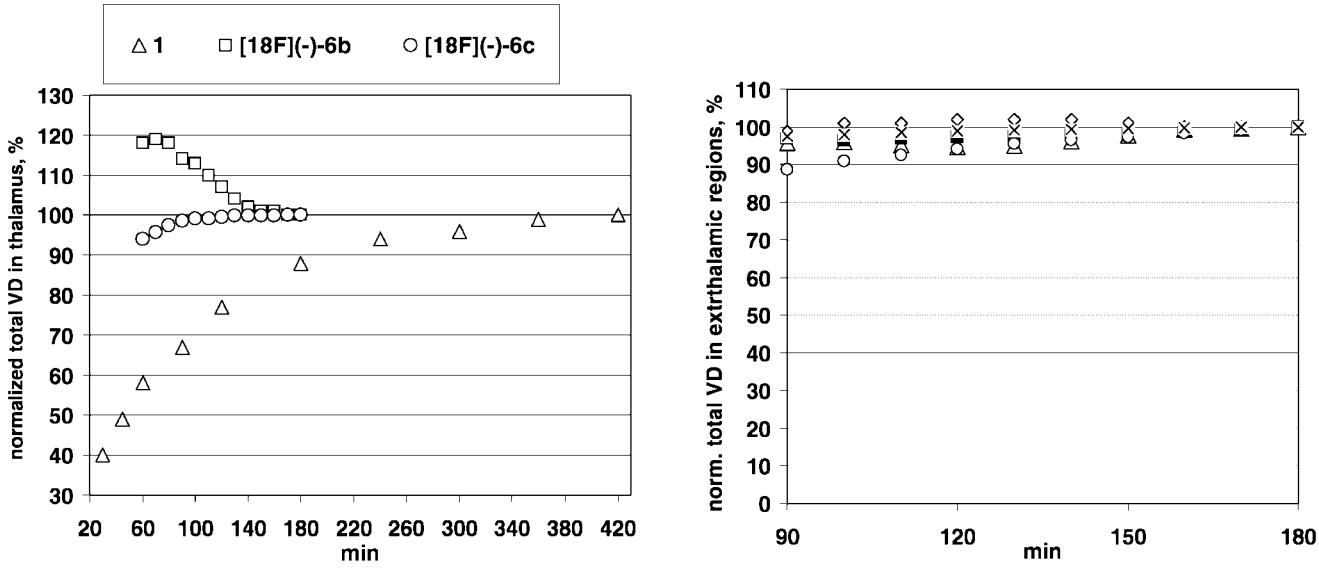

Figure 6. (Left panel) Comparison of effect of the duration of scanning period on the normalized thalamic VD values: **1** (triangles, Rhesus monkey),[46] [^{18}F](−)-**6b** (squares, baboon), and [^{18}F](−)-**6c** (circles, baboon). The data demonstrate that 2−2.5 h and 1−1.5 h of PET scanning are required for accurate estimation of thalamic VD with [^{18}F](−)-**6b** and [^{18}F](−)-**6c**, respectively. **1**, the currently conventional PET radioligand for nAChR imaging, requires at least 5−6 h of PET scanning for accurate estimation of thalamic VD in Rhesus monkey[46] and even longer (see Table 3) in baboon[44] and humans.[45] (Right panel) Comparison of effect of the duration of scanning period on the normalized VD values in the baboon extrathalamic brain regions. Symbols are as follows: triangles = [^{18}F](−)-**3** (frontal cortex); solid squares = [^{18}F](−)-**6a** (frontal cortex); diamonds = [^{18}F](−)-**6b** (frontal cortex); circles = [^{18}F](−)-**6c** (frontal cortex); crosses = [^{18}F](−)-**6c** (basal ganglia). The data of this panel demonstrate that about 1.5 h of scanning is sufficient for accurate estimation of extrathalamic VD with all four radioligands.

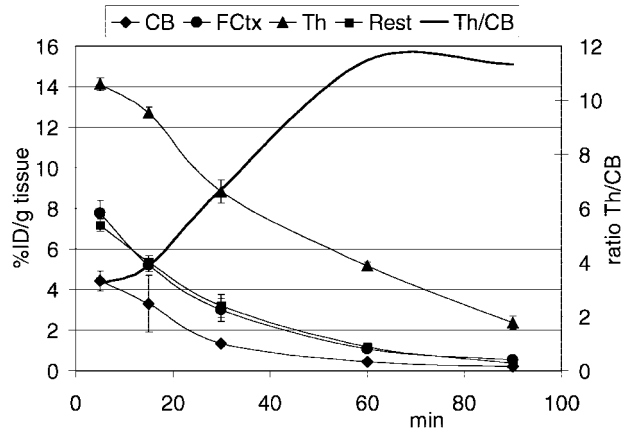

Figure 7. Regional brain distribution of [^{18}F](−)-**6c** in the mouse brain: CB = cerebellum, FCtx = frontal cortex, Th = thalamus. Data = mean ± SD (n = 3).

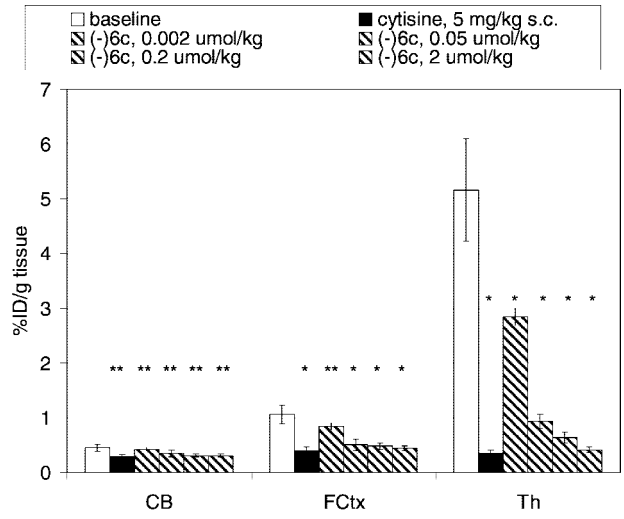

Figure 8. Comparison of regional brain uptake of [^{18}F](−)-**6c** in mice at 60 min time point in control and blocking experiments with selective α4β2-agonist cytisine (5 mg/kg, sc) and various iv doses of unlabeled (−)-**6c** (0.002−2 μmol/kg, iv): CB = cerebellum, FCtx = frontal cortex,Th = thalamus. Data = mean ± SD (n = 3): (*) $P < 0.01$, significantly different from controls; (**) $P > 0.01$, insignificantly different from controls (ANOVA single-factor analysis).

accumulation of [^{18}F](−)-**6c** in the thalamus (14.1 ± 1.7% of injected dose per gram of tissue (%ID/g tissue, mean ± SD (n = 3)), the region with highest density of nAChR, was seen at 5 min after injection followed by washout. The initial clearance rate [^{18}F](−)-**6c** from the nAChR-poor cerebellum was higher than that from all other regions studied. Therefore, tissue-to-cerebellar ratios increased steadily over the initial observation period after injection, reaching value of 12 in thalamus (Figure 7) at 1 h after tracer administration.

Subcutaneous preadministration of cytisine, a selective α4β2-nAChR ligand, significantly inhibited [^{18}F](−)-**6c** binding at 60 min after tracer administration in the mouse thalamus and cortex, but inhibition was not significant in cerebellum (Figure 8). This finding proves that specific binding of [^{18}F](−)-**6c** in the mouse brain is nAChR-mediated, and the observed accumulation of radioactivity is consistent with regional distribution of nAChR in the mammalian brain.

In a separate study unlabeled (−)-**6c** (0.002−2 μmol/kg, iv) was injected before administration of [^{18}F](−)-**6c** to study saturation of in vivo binding. A significant dose-dependent reduction of radioactivity of [^{18}F](−)-**6c** by blockade with (−)-**6c** was observed in the nAChR-rich brain regions studied here but not in the nAChR-poor cerebellum (Figure 8). The values of specific binding in thalamus (94%) and frontal cortex (71%) were estimated using the radioactivity concentration in the blocked cerebellum as nonspecific binding.

All intravenous doses of "cold" (−)-**6c** (0.002−2 μmol/kg) (Figure 8) produced in mice little sign of toxicity (Table 5). Importantly, the only PET nAChR ligands that are presently used for human studies, **1**[29,30] and **2**,[31] have demonstrated side effects at a similar dose range (Table 5). It is noteworthy that we did not observe Straub tail[32] in mice after injection of iv doses of (−)-**6c** (0.002−0.2 μmol/kg). This finding suggests that at this dose range compound (−)-**6c** does not display in vivo functional properties of an nAChR agonist. Most available PET and SPECT imaging agents are nAChR agonists. These nAChR agonists are toxic when injected at high doses.[29,30,33] In the functional assay (Figure 3) (−)-**6c** exhibited properties of an α4β2-nAChR antagonist, and the few side effects of (−)-**6c** in mice support those results of the functional assay.

The preliminary assessment of toxicological properties of (−)-**6c** demonstrated that (−)-**6c** exhibits a lower toxicity than **1** and **2** and merits further development as a potential PET radioligand for human subjects.

Conclusion

A series of isomers of 7-methyl-2-*exo*-[3′-([^{18}F]fluoropyridinyl)-5′-pyridinyl]-7-azabicyclo[2.2.1]heptane with a picomolar range of binding affinities have been developed as potential radioligands with optimized brain kinetics for quantitative PET imaging of nAChRs. Two compounds of the series, isomers [^{18}F](−)-**6b** and [^{18}F](−)-**6c**, have demonstrated remarkable properties as superb radioligands for PET imaging of nAChRs.

Compound [^{18}F](−)-**6b** ((−)-7-methyl-2-*exo*-[3′-(2-[^{18}F]fluoropyridin-3-yl)-5′-pyridinyl]-7-azabicyclo[2.2.1]heptane) is an excellent radioligand for PET imaging of extrathalamic nAChR with high BP values and improved brain kinetics that are superior to the previously developed extrathalamic radioligands and merits further investigation.

Unlike any other nAChR radioligands that we are aware of, including the nAChR radioligands developed by our group (about 70) and others, (−)-7-methyl-2-*exo*-[3′-(6-[^{18}F]fluoropyridin-2-yl)-5′-pyridinyl]-7-azabicyclo[2.2.1]heptane, [^{18}F](−)-**6c**, exhibits a unique combination of the optimally rapid brain kinetics, favorable metabolic profile, and high BPs. For comparison, all nAChR radioligands previously developed by us and others with similarly rapid kinetics exhibited low BP[7–9,11,34,35] and, vice versa, radioligands with similarly high BP values were very "slow".[12] In addition to these excellent imaging properties [^{18}F](−)-**6c**, an antagonist of α4β2-nAChR (Figure 3), displays even fewer side effects in mice than **1** and **2**. What is more, [^{18}F](−)-**6c** exhibits a substantially greater total brain uptake than **1** (600% SUV versus 150% SUV), suggesting that a lower dose of [^{18}F](−)-**6c** would be required for a PET study and therefore [^{18}F](−)-**6c** is likely to give a lower radiation burden to animals and human research subjects.

This combination of imaging properties suggests that [^{18}F](−)-**6c** is a potentially superior replacement for **1** and **2**, currently the only available nAChR PET radioligands for human studies.

Because of the high stakes of development of new PET radioligand for humans, there is a need for additional animal experiments with [^{18}F](−)-**6b** and [^{18}F](−)-**6c** that will include test/retest PET studies in baboon, rodent pharmacology, including blocking studies with non-nAChR CNS ligands, radiation dosimetry, and toxicology. These substantial animal studies, as

Table 5. Comparison of Preliminary Acute Toxicity in CD-1 Mice (Three Animals per Dose) of (−)-**6c** with **1** and **2**, PET Ligands for Imaging of nAChR in Humans[a]

drug	drug dose, μmol/kg (iv)/effect				
1[29,30]	0/ne[b]	0.8/Straub tail, circling behavior	1.7/Straub tail, circling behavior	3.3/Straub tail, hyperactivity	6.7/Straub tail, seizures
2[31]	0/ne[b]	1.3/Straub tail, seizures	2.0/death		
(−)-**6c**	0/ne[b]	0.002/ne[b]	0.05/ne[b]	0. 2/ne[b]	2.0/ne[b,c]

[a] The data were obtained in the blockade experiments (Figure 7). Note: the common mass-dose range of PET radiotracers in humans is 0.2−0.5 nmol/kg. [b] ne = no effect observed. [c] Reduced locomotor activity and initial Straub tail with full recovery in 10 min after injection.

well as optimization of chemistry and radiochemistry of [^{18}F](−)-**6b** and [^{18}F](−)-**6c**, are well beyond the scope of this paper but are currently in progress by our group.

Experimental Section

All reagents were used directly as obtained commercially unless otherwise noted. Compounds **9** and **22** were purchased from Alfa Aesar. Compound **12** was from Frontier Scientific Inc., and compound **13** was from Matrix Scientific Inc. All other reagents were purchased from Aldrich Chemical Co., Inc.

Column flash chromatography was carried out using E. Merck silica gel 60F (230−400 mesh). Analytical thin-layer chromatography (TLC) was performed on aluminum sheets coated with silica gel 60 F_{254} (0.25 mm thickness, E. Merck, Darmstadt, Germany). Melting points were determined with a Fisher−Johns apparatus and were not corrected. ^{1}H NMR and ^{13}C NMR spectra were recorded with a Varian-400 NMR spectrometer at nominal resonance frequencies of 400 and 100 MHz, respectively, in $CDCl_3$ (referenced to internal Me_4Si at δ_H 0 ppm, δ_C 0 ppm). The chemical shifts (δ) were expressed in parts per million (ppm). First order J values were given in hertz. High resolution mass spectrometry was performed at the University of Notre Dame Mass Spectrometry facility. Elemental analyses were determined by Galbraith Laboratories, Inc. (Knoxville, TN). The HPLC system consisted of two Waters model 600 pumps, two Rheodyne model 7126 injectors, an in-line Waters model 441 UV detector (254 nm), and a single sodium iodide crystal flow radioactivity detector. All HPLC chromatograms were recorded with Varian Galaxy software (version 1.8). The analytical and semipreparative chromatographies were performed using Phenomenex Luna C-18 10 μm columns (analytical 4.6 mm × 250 mm and semipreparative 10 mm × 250 mm). The racemic compounds were separated into their enantiomers by chiral HPLC, using a Chiralcel-OD column, 250 mm × 20 mm (Daicel Chemical Industries, Ltd.) and a mixture of 2-propanol/hexane/triethylamine or 2-propanol/hexane/diethylamine, as an eluent, at a flow rate of 4 mL/min. The purity of enantiomers (+)-**6c** and (−)-**6c** was checked by different chiral HPLC using Regis column (analytical 4.6 mm × 250 mm, Regis Technologies, Inc.) and a mixture of ethanol/hexane/diethylamine, as an eluent, at a flow rate of 2 mL/min.

A dose calibrator (Capintec 15R) was used for all radioactivity measurements. Radiofluorination was performed with a modified GE FDG radiochemistry box.

Chemistry. 7-*tert*-Butoxycarbonyl-2-*exo*-[3′-(2-fluoropyridin-4-yl)-5′-pyridinyl]-7-azabicyclo[2.2.1]heptane, 10a. A solution of 2-(5-bromopyridin-3-yl)-7-*tert*-buthoxycarbonyl-7-azabicyclo[2.2.1]heptane **7**[13] (113 mg, 0.32 mmol), 2-fluoro-4-(trimethylstannyl)pyridine **8**,[14] (125 mg, 0.48 mmol), and tetrakis(triphenylphosphine)palladium(0) (23.8 mg, 0.021 mmol) was heated and stirred at 115−120 °C for 9 h in anhydrous toluene (3 mL). The reaction was monitored by TLC (1:1 hexanes/ethyl acetate). The solvent was then evaporated at 50−60 °C. Final purification was done by gradient flash column chromatography (5:1 to 3:2 hexane/ethyl acetate). The product was obtained as an oil (85 mg, 72%). ^{1}H NMR (400 MHz, $CDCl_3$/TMS) δ 8.73 (d, J = 1.6 Hz, 1H), 8.58 (d, J = 1.6 Hz, 1H), 8.31 (d, J = 5.2 Hz, 1H), 7.94 (m, 1H), 7.42 (m, 1H), 7.15 (m, 1H), 4.42 (s, 1H), 4.29 (s, 1H), 2.98 (dd, J = 5.0 Hz, 9.0 Hz, 1H), 2.04 (dd, J = 9.2 Hz, 12.4 Hz, 1H), 1.86−1.91 (m, 2H), 1.58−1.71 (m, 3H), 1.44 (s, 9H); HRMS calculated for $C_{21}H_{25}FN_3O_2$, [M + H] m/z = 370.1932; found, 370.1940.

2-*exo*-[3′-(2-Fluoropyridin-4-yl)-5′-pyridinyl]-7-azabicyclo[2.2.1]-heptane, 11a. A solution of **10a** (75 mg, 0.2 mmol) in methylene chloride (3 mL) and trifluoroacetic acid (0.22 mL) was stirred at room temperature for 1.5 h. The organic solvents were removed by evaporation. The residue was treated with 15 mL of ammonium hydroxide and extracted with $CHCl_3$ (3 × 20 mL). The solvent evaporated and the residue was purified by silica gel column chromatography using $CHCl_3$/EtOH 10:1 to 1:1 as eluent to give the product as a colorless oil (52 mg, 96%). ^{1}H NMR (400 MHz, $CDCl_3$/TMS) δ 8.70 (d, J = 2.0 Hz, 1H), 8.62 (d, J = 2.0 Hz, 1H), 8.31 (d, J = 5.2 Hz, 1H), 8.07 (m, 1H), 7.43 (m, 1H), 7.17 (m, 1H), 3.87 (m, 1H), 3.67 (br s, 1H), 2.88 (dd, J = 5.0 Hz, 9.0 Hz, 1H), 1.93−2.01 (m, 2H), 1.86−1.91 (m, 2H), 1.56−1.77 (m, 5H).

7-*tert*-Butoxycarbonyl-2-*exo*-[3′-(2-fluoropyridin-3-yl)-5′-pyridinyl]-7-azabicyclo[2.2.1]heptane, 10b. To a resealable reaction vessel under nitrogen were added **7** (178 mg, 0.504 mmol), $Pd(PPh_3)_4$ (58 mg, 0.05 mmol), sodium carbonate (107 mg, 1.01 mmol), and 2-fluoro-3-pyridinylboronic acid **9** (114 mg, 0.81 mmol), degassed (nitrogen bubbling) water (1 mL), and dimethoxyethane (5 mL). The mixture was heated at 80 °C for 20 h, cooled, poured into 60 mL of saturated $NaHCO_3$, extracted with ethyl acetate (4 × 30 mL), and evaporated to dryness. The residue was purified by flash chromatography (initially 1:1 ethylacetate/hexanes, then 2:1 ethylacetate/hexanes) to give the product as a white solid (135 mg, 72%). ^{1}H NMR (400 MHz, $CDCl_3$/TMS) δ 8.65 (br s, 1H), 8.53 (d, J = 2.0 Hz, 1H), 8.25 (d, J = 4.8 Hz, 1H), 7.88 (m, 1H), 7.68 (m, 1H), 7.32 (m, 1H), 4.41 (br s, 1H), 4.27 (br s, 1H), 2.97 (dd, J = 4.8 Hz, 8.8 Hz, 1H), 2.06 (dd, J = 8.8 Hz, 12.4 Hz, 1H), 1.88−1.92 (m, 3H), 1.55−1.62 (m, 2H), 1.43 (s, 9H); HRMS calculated for $C_{18}H_{18}FN_4$, [M + H] m/z = 370.1931; found, 370.1940.

2-*exo*-[3′-(2-Fluoropyridin-3-yl)-5′-pyridinyl]-7-azabicyclo[2.2.1]-heptane, 11b. A solution of **10b** (65 mg, 0.16 mmol) in CH_2Cl_2 (3 mL) and trifluoroacetic acid (0.22 mL) was stirred at room temperature for 1.5 h. The organic solvents were removed by evaporation. The residue was treated with a 3:1 mixture of ammonium hydroxide−water (15 mL) and extracted with $CHCl_3$ (3 × 20 mL). The solvent evaporated and the residue was purified by silica gel column chromatography using $CHCl_3$/EtOH 10:1 to 1:1 as eluent to give the product as a colorless oil (40 mg, 93%). ^{1}H NMR (400 MHz, $CDCl_3$/TMS) δ 8.63 (brs, 1H), 8.58 (br s, 1H), 8.25 (m, 1H), 7.95 (br s, 1H), 7.91 (m, 1H), 7.32 (m, 1H), 3.86 (s, 1H), 3.69 (s, 1H), 2.90 (dd, J = 5.2 Hz, 8.8 Hz, 1H), 2.19 (br s, 2H), 1.99 (dd, J = 9.2 Hz, 12.4 Hz, 1H), 1.53−1.79 (m, 4H).

5′-Bromo-6-fluoro-2,3′-bipyridine, 14. 2-Bromo-6-fluoropyridine **13** (620 mg, 3.5 mmol), 3-bromopyridine-5-boronic acid **12** (920 mg, 4.55 mmol), and potassium carbonate (970 mg, 7 mmol) were dissolved in 25 mL of toluene, 3 mL of EtOH, 3 mL of H_2O. This mixture was purged of oxygen and refilled with argon. Then $Pd(Ph_3P)_4$ (200 mg, 0.17 mmol) was added to the mixture, and the mixture was heated to 90−95 °C for 5 h. Water (30 mL) was then added to the reaction mixture, and the organic layer was partitioned. The aqueous layer was extracted with ethyl acetate (2 × 50 mL), and the combined organic layers were dried with Na_2SO_4 and concentrated. The residue was purified by column chromatography (hexanes/ethyl acetate 3:1) to give a white solid (700 mg, 79%). ^{1}H NMR (400 MHz, $CDCl_3$/TMS) δ 9.09 (d, J = 2.0 Hz, 1H),

8.72 (d, $J = 2.4$ Hz, 1H), 8.51 (m, 1H), 7.92 (dd, $J = 8.0$ Hz, 16.0 Hz, 1H), 7.67 (dd, $J = 2.4$ Hz, 8.0 Hz, 1H), 6.97 (dd, $J = 2.4$ Hz, 8.0 Hz, 1H).

7-*tert*-Butoxycarbonyl-2-*exo*-[3′-(6-fluoropyridin-2-yl)-5′-pyridinyl]-7-azabicyclo[2.2.1]heptane, 10c. A mixture of 7-*tert*-butoxycarbonyl-7-aza-bicyclo[2.2.1]hept-2-ene**15** (68 mg, 0.35 mmol), **14** (177 mg, 0.7 mmol) $Pd(PPh_3)_4$ (61 mg, 0.053 mmol), piperidine (0.081 mL, 0.82 mmol), formic acid (0.027 mL, 0.7 mmol), and DMF (1 mL) was stirred in a sealed vial at 80 °C for 46 h. The solvent was removed in vacuo and the residue was treated with $CHCl_3$ (100 mL). The organic phase was washed with brine, dried (Na_2SO_4), and concentrated. The residue was purified by chromatography with hexane/ethyl acetate (1:1) to give an oil (93 mg, 72%). ^{1}H NMR (400 MHz, $CDCl_3$/TMS) δ 9.0 (s 1H), 8.57 (s, 1H), 8.26 (m, 1H), 7.87 (dd, $J = 8.0$ Hz, 16 Hz, 1H), 7.67 (dd, $J = 2.4$ Hz, 8.0 Hz, 1H), 6.92 (dd, $J = 2.8$ Hz, 8.0 Hz, 1H), 4.43 (s, 1H), 4.29 (s, 1H), 2.98 (dd, $J = 5.0$ Hz, 9.0 Hz, 1H), 2.04 (dd, $J = 8.8$ Hz, 12 Hz, 1H), 1.87−1.95 (m, 3H), 1.54−1.69 (m, 2H), 1.43 (s, 9H).

2-*exo*-[3′-(6-Fluoropyridin-2-yl)-5′-pyridinyl]-7-azabicyclo[2.2.1]-heptane, 11c. A solution of **10c** (25 mg, 0.07 mmol) in CH_2Cl_2 (1 mL) and trifluoroacetic acid (0.1 mL) was stirred at room temperature for 1.5 h. The organic solvents were removed by evaporation. The residue was treated with 15 mL of a mixture of ammonium hydroxide/water (3:1) and extracted with $CHCl_3$ (3 × 20 mL). The solvent evaporated and the residue was purified by silica gel column chromatography using $CHCl_3$/EtOH 10:1 to 1:1 as eluent to give the product as an oil (17 mg, 90%). ^{1}H NMR (400 MHz, $CDCl_3$/TMS) δ 8.99 (d, $J = 2.0$ Hz, 1H), 8.60 (d, $J = 2.0$ Hz, 1H), 8.33 (m, 1H), 7.87 (dd, $J = 8.0$ Hz, 16 Hz, 1H), 7.67 (dd, $J = 2.4$ Hz, 8.0 Hz, 1H), 6.92 (dd, $J = 3.2$ Hz, 8.4 Hz, 1H), 3.84 (m, 1H), 3.66 (m, 1H), 2.92 (dd, $J = 5.0$ Hz, 9.0 Hz, 1H), 1.96 (dd, $J = 8.8$ Hz, 12 Hz, 1H), 1.74−1.80 (m, 1H), 1.53−1.67 (m, 5H).

General Procedures for Preparing Tertiary Amines, (±)-6a, (±)-6b, (±)-6c, (+)-6c, and (−)-6c. The secondary amine ((±)-**11a**, (±)-**11b**, (±)-**11c**, (+)-**11c**, or (−)-**11c**)(0.14 mmol) was dissolved in 1 M sodium phosphite solution (2.5 mL). Aqueous formaldehyde (37%) (0.22 mL) was added, and the reaction mixture was heated with stirring at 60 °C for 30 min. The reaction flask was cooled, and 5% K_2CO_3 (25 mL) was added. The mixture was extracted with $CHCl_3$ (4 × 20 mL). The $CHCl_3$ extracts were dried over sodium sulfate, filtered, and evaporated to give a residue that was purified by silica gel chromatography ($CHCl_3$/MeOH 15:1 to 5:1), revealing tertiary amines (±)-**6a**, (±)-**6b**, (±)-**6c**, (+)-**6c**, or (−)-**6c**).

(±)-7-Methyl-2-*exo*-[3′-(2-fluoropyridin-4-yl)-5′-pyridinyl]-7-azabicyclo[2.2.1]heptane, (±)-6a. The reagent was compound **11a.**The product was obtained as a colorless oil with yield of 95%. ^{1}H NMR (400 MHz, $CDCl_3$/TMS) δ 8.69 (s, 1H), 8.65 (d, $J = 2.0$ Hz, 1H), 8.31 (d, $J = 5.2$ Hz, 1H), 8.14 (m, 1H), 7.43 (m, 1H), 7.16 (br s, 1H), 3.37 (m, 1H), 3.22 (br s, 1H), 2.76 (dd, $J = 5.0$ Hz, 9.0 Hz, 1H), 2.29 (s, 3H), 1.77−1.98 (m, 4H), 1.48 (m, 2H); HRMS calculated for $C_{17}H_{19}FN_3$ [M + H] $m/z = 284.1564$; found 284.1563; Anal. ($C_{17}H_{18}FN_3 \cdot 0.3H_2O$) C, H, N.

(±)-7-Methyl-2-*exo*-[3′-(2-fluoropyridin-3-yl)-5′-pyridinyl]-7-azabicyclo[2.2.1]heptane, (±)-6b. The reagent was compound **11b**. The product was obtained as a colorless oil with yield of 88%. ^{1}H NMR (400 MHz, $CDCl_3$/TMS) δ 8.60 (br s 2H), 8.25 (m, 1H), 8.08 (m, 1H), 7.87−7.92 (m, 1H), 7.32 (m, 1H), 3.35 (m, 1H), 3.25 (m, 1H), 2.76 (dd, $J = 5.2$ Hz, 9.6 Hz, 1H), 2.27 (s, 3H), 1.87−1.92 (m, 2H), 1.75 (m, 2H), 1.41−1.47 (m, 2H); HRMS calculated for $C_{17}H_{19}FN_3$, [M + H] $m/z = 284.1564$; found, 284.1563; Anal. ($C_{17}H_{18}FN_3 \cdot 0.2H_2O$) C, H, N.

(±)-7-Methyl-2-*exo*-[3′-(6-fluoropyridin-2-yl)-5′-pyridinyl]-7-azabicyclo[2.2.1]heptane, (±)-6c. The reagent was compound **11c**. The product was obtained as a colorless oil. The yield was 92%. ^{1}H NMR (400 MHz, $CDCl_3$/TMS) δ 8.98 (d, $J = 2.4$ Hz, 1H), 8.60 (d, $J = 2.4$ Hz, 1H), 8.38 (m, 1H), 7.88 (dd, $J = 8.0$ Hz, 16 Hz, 1H), 7.66 (dd, $J = 2.2$ Hz, 8.0 Hz, 1H), 6.92 (dd, $J = 3.2$ Hz, 8.4 Hz, 1H), 3.37 (m, 1H), 3.28 (m, 1H), 2.78 (dd, $J = 5.0$ Hz, 9.0 Hz, 1H), 2.29 (s, 3H), 1.81−1.98 (m, 4H), 1.47 (m, 1H); HRMS calculated for $C_{17}H_{19}FN_3$, [M + H] $m/z = 284.1563$; found, 284.1585. Anal. ($C_{17}H_{18}FN_3$) C, H, N.

(−)-7-Methyl-2-*exo*-[3′-(6-fluoropyridin-2-yl)-5′-pyridinyl]-7-azabicyclo[2.2.1]heptane, (−)-6c. The reagent was compound (+)-**11c**. The product was obtained as a colorless oil. The yield was 90%. ^{1}H NMR (400 MHz, $CDCl_3$/TMS) δ 8.98 (d, $J = 2.4$ Hz, 1H), 8.60 (d, $J = 2.4$ Hz, 1H), 8.38 (m, 1H), 7.88 (dd, $J = 8.0$ Hz, 16 Hz, 1H), 7.66 (dd, $J = 2.2$ Hz, 8.0 Hz, 1H), 6.92 (dd, $J = 3.2$ Hz, 8.4 Hz, 1H), 3.37 (m, 1H), 3.28 (m, 1H), 2.78 (dd, $J = 5.0$ Hz, 9.0 Hz, 1H), 2.29 (s, 3H), 1.81−1.98 (m, 4H), 1.47 (m, 1H). Anal. ($C_{17}H_{18}FN_3 \cdot 0.1H_2O$) C, H, N.

(+)-7-Methyl-2-*exo*-[3′-(6-fluoropyridin-2-yl)-5′-pyridinyl]-7-azabicyclo[2.2.1]heptane, (+)-6c. The reagent was compound (−)-**11c**. The product was obtained as a colorless oil. The yield was 95%. ^{1}H NMR (400 MHz, $CDCl_3$/TMS) δ 8.98 (d, $J = 2.4$ Hz, 1H), 8.60 (d, $J = 2.4$ Hz, 1H), 8.38 (m, 1H), 7.88 (dd, $J = 8.0$ Hz, 16 Hz, 1H), 7.66 (dd, $J = 2.2$ Hz, 8.0 Hz, 1H), 6.92 (dd, $J = 3.2$ Hz, 8.4 Hz, 1H), 3.37 (m, 1H), 3.28 (m, 1H), 2.78 (dd, $J = 5.0$ Hz, 9.0 Hz, 1H), 2.29 (s, 3H), 1.81−1.98 (m, 4H), 1.47 (m, 1H). Anal. ($C_{17}H_{18}FN_3$) C, H, N.

7-*tert*-Butoxycarbonyl-2-*exo*-[3′-(2-bromopyridin-4-yl)-5′-pyridinyl]-7-azabicyclo[2.2.1]heptane, 18a. 2-(5-Iodopyridin-3-yl)-7-*tert*-buthoxycarbonyl-7-aza-bicyclo[2.2.1]heptane **16** (71 mg, 0.18 mmol), 2-bromo-4-trimethyltinpyridine **17** (78 mg, 0.243 mmol, 1.35 equiv), and tetrakis(triphenylphosphine)palladium(0) (21 mg, 0.02 mmol) were dissolved in anhydrous toluene (2 mL). The mixture was heated in a sealed reaction vessel and stirred at 110 °C for 20 h. TLC (1:1 hexanes/ethyl acetate) was used to monitor the reaction process. The solvent was then evaporated at 50−60 °C. Final purification was done by gradient flash column chromatography (hexane/acetone 4:1 to 1:1). The product was obtained as yellow oil (38 mg, 49%). ^{1}H NMR (400 MHz, $CDCl_3$/TMS) δ 8.70 (d, $J = 1.6$ Hz, 1H), 8.57 (d, $J = 2.0$ Hz, 1H), 8.45 (d, $J = 5.2$ Hz, 1H), 7.91 (br s, 1H), 7.70 (br s, 1H), 7.48 (m, 1H), 4.42 (s, 1H), 4.28 (s, 1H), 2.98 (dd, $J = 4.8$ Hz, 8.8 Hz, 1H), 2.06 (m, 1H), 1.56−1.89 (m, 5H), 1.44 (s, 9H); HRMS calculated for $C_{21}H_{25}BrN_3O_2$, [M + H] $m/z = 430.1131$; found 430.1146.

2-*exo*-[3′-(2-Bromopyridin-4-yl)-5′-pyridinyl]-7-azabicyclo[2.2.1]-heptane, 19a. The mixture of **18a** (43 mg, 0.1 mmol), CH_2Cl_2 (5 mL), and TFA (1 mL) was stirred at ambient temperature for 3 h until the reaction was complete. The solvent was evaporated to dryness. The residue was treated with a 3:1 mixture of ammonium hydroxide/water (15 mL) and extracted with $CHCl_3$ (3 × 20 mL). The solvent was evaporated and the residue was purified by silica gel column chromatography using $CHCl_3$/EtOH 10:1 to 1:1 as eluent to give **19a** as oil (33 mg, 100%). ^{1}H NMR (400 MHz, $CDCl_3$/TMS) δ 8.67 (d, $J = 2.4$ Hz, 1H), 8.62 (d, $J = 2.4$ Hz, 1H), 8.45 (d, $J = 5.2$ Hz, 1H), 8.03 (t, $J = 2.0$ Hz, 1H), 7.71 (m, 1H), 7.48 (dd, $J = 1.6$ Hz, 5.2 Hz, 1H), 3.85 (m, 1H), 3.64 (br s, 1H), 2.86 (dd, $J = 4.8$ Hz, 8.8 Hz, 1H), 1.96 (dd, $J = 8.8$ Hz, 12.4 Hz, 1H), 1.56−1.74 (m, 6H).

2-Amino-5′-bromo-3,3′-bipyridine, 23. 2-Amino-3-iodopyridine **21** (495 mg, 2.25 mmol), 3-bromopyridine-5-boronic acid **12** (635 mg, 3.15 mmol, 1.4 equiv), and potassium carbonate (622 mg, 4.5 mmol, 2 equiv) were dissolved in 20 mL of tolune, 2 mL of EtOH, 2 mL of H_2O. This mixture was purged of oxygen and refilled with argon. Then $Pd(Ph_3P)_4$ (130 mg, 0.112 mmol, 5%mol) was added to the mixture, and the mixture was heated to 90 °C for 22 h. Water (25 mL) was then added to the reaction mixture, and the organic layer was partitioned. The aqueous layer was extracted with ethyl acetate (2 × 40 mL), and the combined organic layers were dried with Na_2SO_4 and concentrated. The crude reaction product was triturated with Et_2O (6 mL) and filtered. The resulting solid was collected (180 mg). The Et_2O solution was evaporated and applied to silica gel and eluted with $CHCl_3$/MeOH 50:1 to 20:1 to give another aliquot 276 mg. Yield: 81%. ^{1}H NMR (400 MHz, $CDCl_3$/TMS) δ 8.69 (d, $J = 2.4$ Hz, 1H), 8.63 (d, $J = 2.0$ Hz, 1H), 8.13 (dd, $J = 1.6$ Hz, 5.0 Hz, 1H), 7.98 (m, 1H), 7.36 (dd, $J = 1.6$ Hz, 7.6 Hz, 1H), 6.79 (dd, $J = 5.0$ Hz, 7.6 Hz, 1H), 4.63 (br s, 2H).

7-*tert*-Butoxycarbonyl-2-*exo*-[3′-(2-aminopyridin-3-yl)-5′-pyridinyl]-7-azabicyclo[2.2.1]heptane, 18b. To a resealable reaction vessel containing degassed DMF (1 mL) were added **15** (98 mg, 0.51 mmol), **23** (190 mg, 0.76 mmol), *n*-Bu_4NCl (36 mg, 0.13 mmol), KO_2CH (68 mg, 0.8 mmol), and $Pd(OAc)_2$ (15 mg, 0.065 mmol). The reaction vessel was inserted into a 100−105 °C oil bath. After 68 h, the reaction mixture was diluted with 30 mL of ethyl acetate and filtered through a Celite pad into 30 mL of 1:1 NH_4OH and water. The aqueous phase was extracted with ethyl acetate (3 × 40 mL). The combined organic phase was dried (Na_2SO_4), filtered, and concentrated under reduced pressure. The resulting brown oil was purified by column chromatography, eluting with hexanes/ethyl acetate (1:1) to give the product (78 mg, 42%). ^{1}H NMR (400 MHz, $CDCl_3$/TMS) δ 8.54 (d, J = 2.0 Hz, 1H), 8.50 (d, J = 2.0 Hz, 1H), 8.10 (dd, J = 2.0 Hz, 4.8 Hz, 1H), 7.79 (br s, 1H), 7.36 (dd, J = 2.0 Hz, 7.6 Hz 1H), 6.76 (dd, J = 5.2 Hz, 7.6 Hz, 1H), 4.58 (br s, 2H), 4.40 (br s, 1H), 4.24 (br s, 1H), 2.95 (m, 1H), 2.04 (dd, J = 8.8 Hz, 12.4 Hz, 1H), 1.86 (m, 3H), 1.51−1.65 (m, 2H), 1.43 (s, 9H).

2-*exo*-[3′-(2-Bromopyridin-3-yl)-5′-pyridinyl]-7-azabicyclo[2.2.1]heptane, 19b. To a solution of **18b** (114 mg, 0.31 mmol) dissolved in concentrated HBr (48%, 1.5 mL) was added sodium nitrite (400 mg, 5.8 mmol) and CuBr (1 g, 6.95 mmol) at 0 °C. The mixture was stirred overnight at room temperature. The reaction mixture was poured into a 3:1 mixture of water/NH_4OH, extracted with chloroform, dried with sodium sulfate, and concentrated. The residue was purified by flash chromatography on silica gel using a mixture of $CHCl_3$/MeOH (10:1 to 1:1) as eluent to give an oil (51 mg, 50%). ^{1}H NMR (400 MHz, $CDCl_3$/TMS) δ 8.61 (d, J = 2.4 Hz, 1H), 8.55 (d, J = 1.6 Hz, 1H), 8.39 (dd, J = 2.0 Hz, 4.8 Hz, 1H), 7.95 (m, 1H), 7.82 (dd, J = 2.0 Hz, 7.2 Hz, 1H), 7.36 (dd, J = 4.8 Hz, 7.6 Hz, 1H), 4.20 (br s, 1H), 4.10 (br s, 1H), 3.14 (m, 1H), 2.08−2.17 (m, 5H), 1.65−1.82 (m, 2H); HRMS calculated for $C_{16}H_{17}BrN_3$, [M + H] m/z = 330.0607; found, 330.0596.

6-Amino-5′-bromo-2,3′-bipyridine, 24. 2-Amino-6-bromopyridine **22** (510 mg, 2.95 mmol), 3-bromopyridine-5-boronic acid **12** (775 mg, 3.84 mmol, 1.3 equiv), and potassium carbonate (814 mg, 5.9 mmol, 2 equiv) were dissolved in 20 mL of toluene, 2.5 mL of EtOH, 2.5 mL of H_2O. This mixture was purged of oxygen and refilled with argon. Then $Pd(Ph_3P)_4$ (170 mg, 0.15 mmol) was added to the mixture, and the mixture was heated to 90 °C for 22 h. Water (25 mL) was then added to the reaction mixture, and the organic layer was partitioned. The aqueous layer was extracted with ethyl acetate (2 × 40 mL), and the combined organic layers were dried with Na_2SO_4 and concentrated. The crude reaction product was applied to silica gel and eluted with CH_2Cl_2/MeOH 50:1 to 40:1 to give the product (454 mg, 62%). ^{1}H NMR (400 MHz, $CDCl_3$/TMS) δ 9.03 (d, J = 1.6 Hz, 1H), 8.65 (d, J = 2.0 Hz, 1H), 8.44 (m, 1H), 7.52 (t, J = 8.0 Hz, 1H), 7.08 (d, J = 7.6 Hz, 1H), 6.52 (d, J = 8.4 Hz, 1H), 4.65 (br s, 2H).

7-*tert*-Butoxycarbonyl-2-*exo*-[3′-(6-aminopyridin-2-yl)-5′-pyridinyl]-7-azabicyclo[2.2.1]heptane, 18c. A mixture of **15** (68 mg, 0.35 mmol), **24** (175 mg, 0.7 mmol), $Pd(PPh_3)_4$ (60.7 mg, 0.053 mmol), piperidine (0.081 mL, 0.82 mmol), formic acid (0.027 mL, 0.7 mmol), and DMF (1 mL) was stirred in a sealed vial at 80 °C for 46 h. The solvent was removed in vacuo, and the residue was treated with $CHCl_3$ (30 mL). The organic phase was washed with brine, dried (Na_2SO_4), and concentrated. The residue was purified by chromatography with CH_2Cl_2/MeOH (30:1) to give **18c** (68 mg, 53%). ^{1}H NMR (400 MHz, $CDCl_3$/TMS) δ 8.97 (d, J = 2.0 Hz, 1H), 8.51 (d, J = 2.0 Hz, 1H), 8.16 (m, 1H), 7.52 (t, J = 7.6 Hz, 1H), 7.09 (d, J = 7.2 Hz, 1H), 6.50 (d, J = 8.0 Hz, 1H), 4.56 (br s, 2H), 4.42 (br s, 1H), 4.28 (br s, 1H), 2.96 (m, 1H), 2.01 (m, 1H), 1.53−1.95 (m, 5H).

2-*exo*-[3′-(6-Bromopyridin-2-yl)-5′-pyridinyl]-7-azabicyclo[2.2.1]heptane, 19c. To a solution of **18c** (60 mg, 0.16 mmol) in concentrated HBr (48%, 0.71 mL) was added sodium nitrite (188 mg, 2.73 mmol) and CuBr (0.47 g, 3.27 mmol) at 0 °C. The mixture was stirred overnight at room temperature. The reaction mixture was poured into a mixture of water/NH_4OH (3:1), extracted with chloroform, dried with sodium sulfate, and concentrated. The residue was purified by flash chromatography on silica gel using a mixture of $CHCl_3$/MeOH (10:1 to 1:2) as eluent to give an oil (21 mg, 40%). ^{1}H NMR (400 MHz, $CDCl_3$/TMS) δ 8.96 (br s, 1H), 8.62 (br s, 1H), 8.30 (m, 1H), 7.72 9d, J = 8.0 Hz, 1H), 7.63 (t, J = 7.8 Hz, 1H), 7.46 (d, J = 7.6 Hz, 1H), 3.84 (m, 1H), 3.67 (m, 1H), 2.92 (m, 1H), 1.74−1.97 (m, 3H), 1.53−1.79 (m, 4H).

General Procedures for Preparation of the Radiolabeling Precursors (20a−c). The secondary amine (**19a**, **19b**, or **19c**) (0.14 mmol) was dissolved in 1 M sodium phosphite solution (2.5 mL). Aqueous formaldehyde (37%) (0.22 mL) was added, and the reaction mixture was heated with stirring at 60 °C for 30 min in an oil bath. The reaction flask was cooled, and 5% K_2CO_3 (25 mL) was added. The mixture was extracted with $CHCl_3$ (4 × 20 mL). The $CHCl_3$ extracts were dried over sodium sulfate, filtered, and evaporated to give a residue that was purified by silica gel chromatography ($CHCl_3$/MeOH 15:1 to 5:1), revealing tertiary amines **20a**, **20b**, or **20c**, respectively.

7-Methyl-2-*exo*-[3′-(2-bromopyridin-4-yl)-5′-pyridinyl]-7-azabicyclo[2.2.1]heptane (20a). The reagent was compound **19a**. The product was obtained as a colorless oil. The yield was 62%. ^{1}H NMR (400 MHz, $CDCl_3$/TMS) δ 8.65 (m, 2H), 8.45 (d, J = 5.2 Hz, 1H), 8.10 (t, J = 2.0 Hz, 1H), 7.71 (m, 1H), 7.48 (dd, J = 2.0 Hz, 5.6 Hz, 1H), 3.38 (m, 1H), 3.22 (m, 1H), 2.77 (dd, J = 4.8 Hz, 9.2 Hz, 1H), 2.29 (s, 3H), 1.75−1.99 (m, 4H), 1.45−1.50 (m, 2H).

7-Methyl-2-*exo*-[3′-(2-bromopyridin-3-yl)-5′-pyridinyl]-7-azabicyclo[2.2.1]heptane (20b). The reagent was compound **19b**. The product was obtained as a colorless oil. The yield was 69%. ^{1}H NMR (400 MHz, $CDCl_3$/TMS) δ 8.58 (d, J = 2.4 Hz, 1H), 8.46 (d, J = 2.0 Hz, 1H), 8.41 (dd, J = 2.0 Hz, 4.8 Hz, 1H), 8.04 (m, 1H), 7.65 (dd, J = 1.8 Hz, 7.4 Hz, 1H), 7.37 (dd, J = 4.6 Hz, 7.8 Hz, 1H), 3.36 (m, 1H), 3.27 (m, 1H), 2.77 (m, 1H), 2.27 (s, 3H), 1.75−2.0 (m, 4H), 1.42−1.50 (m, 2H); HRMS calculated for $C_{17}H_{19}BrN_3$, [M + H] m/z = 344.0763; found, 344.0752.

7-Methyl-2-*exo*-[3′-(6-bromopyridin-2-yl)-5′-pyridinyl]-7-azabicyclo[2.2.1]heptane (20c). The reagent was compound **19c**. The product was obtained as a colorless oil. The yield was 90%. ^{1}H NMR (400 MHz, $CDCl_3$/TMS) δ 8.96 (d, J = 2.4 Hz, 1H), 8.51 (d, J = 1.6 Hz, 1H), 8.35 (m, 1H), 7.71 (d, J = 7.6 Hz, 1H), 7.63 (t, J = 7.6 Hz, 1H), 7.46 (d, J = 7.6 Hz, 1H), 3.38 (m, 1H), 3.27 (m, 1H), 2.79 (dd, J = 5.2 Hz, 9.0 Hz, 1H), 2.27 (s, 3H), 1.87−1.98 (m, 2H), 1.45−1.82 (m, 4H); HRMS calculated for $C_{17}H_{19}BrN_3$, [M + H] m/z = 344.0762; found, 344.0752.

General Procedures for Resolution of Racemic Compounds of 6a, 6b, 10c, 20a, 20b, and 20c. The racemic compounds of **6a**, **6b**, **10c**, **20a**, **20b**, and **20c** were separated into their (+)- and (−)-enantiomers by chiral HPLC, using a 250 mm × 20 mm CHIRALCEL-OD column, 0.5−1.5 mg per injection; mobile phase is 2-propanol/hexane/triethylamine or 2-propanol/hexane/diethylamine (Table 1) at a flow rate of 4 mL/min.

Radiochemistry. General Procedure. A solution of the [^{18}F]fluoride, 20 mg of 1,10-diaza-4,7,13,16,21,24-hexaoxabicyclo-[8.8.8]hexacosane (Kryptofix 222), and 3.5 mg of K_2CO_3 in 1 mL of 50% aqueous acetonitrile was added to a reaction vessel of a GE [^{18}F]FDG box. The mixture was heated at 120−135 °C under a stream of argon, while water was evaporated azeotropically after the additions of 2.5 mL of CH_3CN. A solution of the bromo precursor (**20a**, **20b**, or **20c**) (3−4 mg) in anhydrous DMSO (0.8 mL) was added to the reaction vessel and heated at 180 °C for 18 min. The reaction mixture was cooled, diluted with 1 mL of water, injected onto the reverse-phase HPLC column (Phenomenex Luna C-18 10 μm column, 10 mm × 250 mm), and eluted with CH_3CN/H_2O/NEt_3 at flow rate of 12 mL/min. The radioactive peak was collected into 50 mL of HPLC water. The water solution was transferred through an activated Waters C-18 Sep-Pak Plus. After the Sep-Pak was washed with 10 mL water, the product was eluted with 1 mL of ethanol into a vial through a 0.2 μM sterile filter into a sterile, pyrogen-free multidose vial and 10 mL of 0.9% saline was added through the same filter. The final product was then analyzed by analytical HPLC (Phenomenex Luna C-18 10 μm column, analytical 4.6 mm × 250 mm) to determine the radio-

chemical purity and specific radioactivity at the time synthesis ended. The total synthesis time including QC was about 60 min.

(−)-7-Methyl-2-*exo*-[3′-(2-[^{18}F]fluoropyridin-4-yl)-5′-pyridinyl]-7-azabicyclo[2.2.1]heptane, [^{18}F](−)-6a. Eluent for preparative HPLC, 30:70:0.1 v/v/v $CH_3CN/H_2O/NEt_3$; retention time of the [^{18}F](−)-**6a**, 16.3 min; radiochemical yield in two runs, 25% and 47% (nondecay-corrected); eluent for analytical HPLC, 30:70 v/v CH_3CN/0.1 M ammonium formate; retention time of the [^{18}F]-**6a**, 3.0 min; radiochemical purity, >98%; specific radioactivity, 15 500 mCi/μmol and 49 500 mCi/μmol.

(−)-7-Methyl-2-*exo*-[3′-(2-[^{18}F]fluoropyridin-3-yl)-5′-pyridinyl]-7-azabicyclo[2.2.1]heptane, [^{18}F](−)-6b. Eluent for preparative HPLC, 34:66:0.1 v/v/v $CH_3CN/H_2O/NEt_3$; retention time of the [^{18}F](−)-**6b**, 11.2 min; radiochemical yield, 35% ± 16% (n = 3) (nondecay-corrected); eluent for analytical HPLC, 20:80 v/v CH_3CN/0.1 M ammonium formate; retention time of the [^{18}F](−)-**6b**, 4.1 min; radiochemical purity, >98%; specific radioactivity 9400 ± 3900 mCi/μmol (n = 4).

(−)-7-Methyl-2-*exo*-[3′-(6-[^{18}F]fluoropyridin-2-yl)-5′-pyridinyl]-7-azabicyclo[2.2.1]heptane, [^{18}F](−)-6c. Eluent for preparative HPLC, 36:64:0.1 v/v/v $CH_3CN/H_2O/NEt_3$; retention time of the [^{18}F](−)-**6c**, 14.5 min; radiochemical yield, 34 ± 13% (n = 8, nondecay-corrected); eluent for analytical HPLC, 35:65 v/v CH_3CN/0.1 M ammonium formate; retention time of [^{18}F](−)-**6c**, 3.5 min; radiochemical purity, >98%; specific radioactivity in the runs with starting dose of [^{18}F]fluoride of 500−1400 mCi, 18 700 ± 4600 mCi/μmol (n = 4).

The enantiomeric purity (> 98% ee) of the final product was determined with chiral HPLC (Regis Pak, 4.6 mm × 250 mm) using the mobile phase ethanol/hexane/Et_2NH (50:950:1): retention time, 9 min, a single peak was observed (see the Supporting Information).

Functional Assay. SH-EP1 cells stably expressing human $\alpha4\beta2$ nicotinic receptors,[20] obtained as a generous gift from Dr. R. Lukas (Barrow Neurological Institute, Phoenix, AZ), were grown on 35 mm dishes in DMEM (Gibco, Gaithersburg, MD) supplemented with 10% heat inactivated horse serum (Gibco), 5% fetal bovine serum (Gibco), 1 mM sodium pyruvate, 100 U/mL penicillin G, 100 μg/mL streptomycin, 0.25 μg/mL amphotericin B, 0.4 mg/mL hygromycin B, and 0.25 mg/mL Zeocin (Gibco) and maintained at 37 °C in an atmosphere of 5% CO_2 saturated with H_2O.

For electrophysiological recording, the cells were used at ambient temperature in Dulbecco's phosphate buffered saline with the following composition (mM): NaCl, 136.9; KCl, 2.68; $MgCl_2$, 0.49; $CaCl_2$, 0.9; KH_2PO_4, 1.47; Na_2HPO_4, 8.1, glucose, 5.55; sucrose, 45.0; pH 7.40. The composition of the patch pipet solution was (mM): Tris phosphate dibasic, 110; Tris base, 28; $MgCl_2$, 2; $CaCl_2$, 0.1; EGTA, 11; $Mg_3(ATP)_2$, 1.8; brought to pH 7.30 with H_3PO_4.[36] The master stock of (−)-**6c** was kept at −20 °C as a 2 mM ethanol solution that was diluted on the day of use. The cells were voltage clamped at −60 mV using an Alembic VE-2 whole cell amplifier (Alembic Instruments, Montreal, Canada) using 100% series resistance compensation. A modified U-tube[37] was used to locally superfuse drugs. Acetylcholine (ACh), with or without (−)-**6c**, was tested for 4.9 s at about 3.5 min intervals. The currents, recorded using pClamp 7.0 software (Axon Instruments Inc., Union City, CA), were filtered (low pass) to 200 Hz and sampled at 1 kHz.

The concentration response curve (Figure 3C) was obtained by interpolating both mean values and variances from Figure 3B at the 20 min time point. The reciprocal variances were used as weights in fitting the mean values to the competitive inhibition curve: $f(b) = ([ACh] + Ka)/([ACh] + K_a + [b]K_a/K_b)$, where [ACh] = 30 μM, K_a = the dissociation constant for ACh, [b] is the concentration of (−)-**6c**, and K_b = the dissociation constant for (−)-**6c**. Fitting the data for the concentration response of ACh at these cells[36] to the activation function $f(a) = [ACh]/(K_a + [ACh])$ yields K_a = 34 μM. Using this value to find K_b by nonlinear regression analysis (MLAB, Civilized Software, Bethesda, MD) yields the smooth curve shown in Figure 3C and K_b = 0.54 ± 0.08 nM.

In Vitro Binding Studies. Binding to Rat Cerebral Cortex Membrane Preparations. The in vitro inhibition binding assays of (**6a**, **6b**, and **6c**) (Table 2) were performed commercially by NovaScreen Biosciences, a Caliper Life Science Co. (Hanover, MD) under conditions similar to those previously published.[16] In brief, rat cortical membranes were incubated with [^{3}H]epibatidine (K_d = 63 pM) at a concentration of 0.1 nM in a buffer consisting of 50 mM Tris, 120 mM NaCl, 5 mM KCl, 2 mM $CaCl_2$, 1 mM $MgCl_2$, 0.003 mM atropine sulfate at pH 7.4 for 150 min at 0 °C. The binding was terminated by rapid vacuum filtration of the assay contents onto GF/C filters presoaked in PEI. Radioactivity trapped onto the filters was assessed using liquid scintillation spectrometry. Nonspecific binding was defined as that remaining in the presence of 20 nM (±)-epibatidine. The assays were done in duplicate at multiple concentrations of the test compounds. Binding assay results were analyzed using a one-site competition model, and IC_{50} curves were generated based on a sigmoidal dose response with variable slope. The K_i values were calculated using the Cheng−Prusoff equation.

Binding to Defined Rat nAChR Subtypes Expressed by Stably Transfected Mammalian Cell Lines. Stably transfected cell lines, tissue culture conditions, membrane preparation procedures, and binding assays were described previously [17,38] Briefly, cultured cells at >80% confluence were removed from their flasks (80 cm^2) with a disposable cell scraper and placed in 10 mL of 50 mM Tris-HCl buffer (pH 7.4, 4 °C). The cell suspension was centrifuged at 10000g for 5 min, and the pellet was collected. The cell pellet was then homogenized in 10 mL buffer with a Polytron homogenizer and centrifuged at 36000g for 10 min at 4 °C. The membrane pellet was resuspended in fresh buffer, and aliquots of the membrane preparation were used for binding assays. The concentration of [^{3}H]epibatidine used was ~500 pM for competition binding assays. Nonspecific binding was assessed in parallel incubations in the presence of 300 μM nicotine. Bound and free ligands were separated by vacuum filtration through Whatman GF/C filters treated with 0.5% polyethylenimine. The filter-retained radioactivity was measured by liquid scintillation counting. Specific binding was defined as the difference between total binding and nonspecific binding. Data from saturation and competition binding assays were analyzed using Prism 4 (GraphPad Software, San Diego, CA).

Animal Studies. Mice Studies. Male, CD-1 mice weighing 25−30 g from Charles River Laboratories (Wilmington, MA) were used for biodistribution studies. The animals were sacrificed by cervical dislocation at various times (three animals per time point) following injection of radioligand [^{18}F]**6c** (~1.5 MBq (~40 μCi), specific radioactivity was about 259 GBq/mol (7000 mCi/μmol, in 0.2 mL saline), into a lateral tail vein. In the blockade experiments cytisine (5 mg/kg, sc) was injected 15 min prior to the radioligand, and the various doses of unlabeled (−)-**6c** (0.002 - 2 μmol/kg, iv) were injected immediately before the radiotracer. The brains were rapidly removed and dissected on ice. The brain regions of interest were weighed, and their radioactivity content was determined in an automated γ-counter, with a counting error below 3%. Aliquots of the injectate were prepared as standards, and their radioactivity content was counted along with the tissue samples. The percentage of injected dose per gram of tissue (%ID/g tissue) was calculated. All experimental protocols were approved by the Animal Care and Use Committee of the Johns Hopkins Medical Institutions.

Baboon PET Experiments. The experimental protocol was approved by the Animal Care and Use Committee of the Johns Hopkins Medical Institutions. Male baboons (*Papio anubis*, 20−33 kg) were studied in baseline control experiments. The animals were fasted for 12 h prior to the PET study. Anesthesia was given initially with intramuscular injection of (10−15 mg/kg) ketamine. The baboon was intubated, and anesthesia was maintained with a constant infusion of propofol at an average flow rate that corresponded to 0.3−0.4 (mg/kg)/h. Circulatory volume was maintained by infusion of isotonic saline. An arterial catheter was inserted for blood sampling. Physiological vital signs including heart

rate, ECG, blood pressure, and oxygen saturation were continuously monitored throughout the study.

The animal was positioned in a high-resolution research tomograph (ECAT HRRT) brain PET scanner (CPS Innovations, Inc., Knoxville, TN). The head of the baboon was fitted with a thermoplastic mask that was then attached to a head holder for reproducible fixation. A 6 min transmission scan with a 1 mCi ^{68}Ge source was initially performed for attenuation correction. Then dynamic PET data were acquired in 3D list mode during a 3 or 4 h period following a bolus injection of the radioligand in a list mode. Arterial blood was sampled rapidly initially and with prolonging intervals throughout the scan.

To analyze the PET images, the SPGR (spoiled gradient) MRI volume was acquired in the same baboon with the Signa 1.5 T scanner (GE Medical Systems, Milwaukee, WI).

Baboon Plasma Metabolite Analysis. Metabolites of [^{18}F]-labeled radioligands in baboon were studied using a general method previously developed for PET radiotracers. Specifically, arterial blood samples were withdrawn at 5, 15, 30, 60, 90, 120, 150, 180, and 240 min intervals up to 240 min after injection, and plasma was analyzed for the presence of the parent radioligands and their radiolabeled metabolites. Briefly, 3 mL of plasma in 8 M urea is passed through a capture column (19 mm × 4.6 mm Strata-X, Phenomenex, Torrance, CA) at 2 mL/min, followed by 1% acetonitrile in water to wash plasma proteins from the column. The effluent from the capture column, containing only highly polar components, flows through a dual BGO detector (Bioscan, Washington, DC). The solvent is then switched to a mixture of 35% acetonitrile/65% 0.1 M aqueous ammonium bicarbonate (2 mL/min) for elution of the radiolabeled components bound to the capture column onto the analytical column (Gemini C18, 4.6 mm × 250 mm, Phenomenex, Torrance, CA).

PET Data Analysis. Volumes of Interest. The volumes of interest (putamen, thalamus, hippocampus, and cerebellum) were defined with SPGR MRI for caudate nucleus. In addition, a VOI template for cortical regions was used.[39] The template was spatially normalized to each baboon's MRI using the spatial normalization routine of SPM2 (http://www.fil.ion.ucl.ac.uk/spm/). Manually defined VOIs and VOIs from the template were transferred to PET space using the PET-to-MRI coregistration parameters using a SPM2 routine for this purpose. The VOIs were applied to PET frames to generate time−radioactivity curves (TACs) of regions.

Compartmental Models. Time-uptake curves of metabolite-corrected arterial plasma data were used for compartmental analysis. Rate constants of the models are (1) K_1 and k_2 for unidirectional blood-to-brain and brain-to-blood clearance rate constants; (2) k_3 and k_4 for $B_{max}k_{on}$ and k_{off}, where k_{on} and k_{off} are unidirectional association and dissociation constants of the radioligand with nAChR, B_{max}, is the density of available nAChR, k_{on}/k_{off} is the affinity ($1/k_D$), and v_0 is the vascular volume in the tissue. The following models were tested to find the best fit model: (A) one-tissue, one-vascular compartmental model with three parameters (K_1, k_2, and v_0) (OTCM-3) and (B) two-tissue, one-vascular compartmental model (thus, four parameters K_1, k_2, k_3, and v_0) (TTCM-4) (i) with dissociation of the ligand from nAChR (thus, five parameters K_1, k_2, k_3, k_4, and v_0), (ii) without constraining the K_1-k_2 ratio (TTCM-5) or constraining the K_1-k_2 ratio to the estimates in a reference region (i.e., the lowest among regions) (TTCM-5C for the constraint). The study indicated that TTCM-5 and TTCM5C described the data best on the basis of Akaike information criteria.[40]

Our work on the baboon baseline study was as follows: (1) regional total distribution volumes (V_T or K_1/k_2 $(1 + k_3/k_4)$) were obtained with TTCM-5 or TTCM-5C. (2) Regional BP values can be obtained as k_3-k_4 ratios with TTMC-5C but not with TTCM-5. We noted a few outliers in BP values obtained with TTCM-5 as the target-reference tissue distribution volume ratio minus 1 ($V_T/V_T^R - 1$, where V_T^R is V_T of the reference region), suggesting less robustness of TTCM-5.

Time Constancies of V_T and BP Estimates. It is generally observed that shorter PET experiments yield biased estimates of V_T compared with longer experiments. Thus, at 90 min, estimates of V_T reached 97% of the respective 180 min V_T values for [^{18}F](−)-**6c** in the baboon thalamus (Figure 6). The results indicated that the outcome variables may be estimated in 90 min experiments with minimal biases.

Tissue Reference Method. In order to accommodate clinical applications, it is essential to eliminate the need for arterial blood sampling. For this reason, we tested the linear version of the simplified reference tissue method with two parameters, MRTM2 and the reference tissue graphical analysis.[41] The study indicated that MRTM2[42] may be applicable to [^{18}F](−)-**6c** using baboon cerebellum as a reference tissue.

Acknowledgment. The authors thank Dr. Ursula Scheffel and Paige Finley for their valuable help with the animal experiments, Robert C. Smoot for radiochemistry assistance, David J. Clough and Karen Edmonds for PET scanner operation, and Dr. Melinda Roberson for administrative assistance. We are grateful to the generous gift of the SH-EP1 cells from Dr. R. Lukas (Barrow Neurological Institute, Phoenix, AZ). We thank Dr. Richard Wahl for fruitful discussions and support. This research was supported in part by the Division of Nuclear Medicine of Johns Hopkins University School of Medicine and by NIH Grant MH079017 (A.G.H.). The National Institute of Mental Health Psychoactive Drug Screening Program (Grant N01 MH32004) supported some of the in vitro studies.

Supporting Information Available: Elemental analysis results for the target compounds and radio/UV HPLC analysis data for [^{18}F](−)-**6c**. This material is available free of charge via the Internet at http://pubs.acs.org.

References

(1) Horti, A. G.; Villemagne, V. L. The quest for Eldorado: development of radioligands for in vivo imaging of nicotinic acetylcholine receptors in human brain. *Curr. Pharm. Des.* **2006**, *12*, 3877–3900.

(2) Horti, A. G.; Koren, A. O.; Ravert, H. T.; Musachio, J. L.; Mathews, W. B.; London, E. D.; Dannals, R. F. Synthesis of a radiotracer for studying nicotinic acetylcholine receptors: 2-[^{18}F]fluoro-3-(2(*S*)-azetidinylmethoxy)pyridine (2-[^{18}F]A-85380). *J. Labelled Compd. Radiopharm.* **1998**, *41*, 309–319.

(3) Scheffel, U.; Horti, A. G.; Koren, A. O.; Ravert, H. T.; Banta, J. P.; Finley, P. A.; London, E. D.; Dannals, R. F. 6-[^{18}F]Fluoro-A-85380: an in vivo tracer for the nicotinic acetylcholine receptor. *Nucl. Med. Biol.* **2000**, *27*, 51–56.

(4) Oishi, N.; Hashikawa, K.; Yoshida, H.; Ishizu, K.; Ueda, M.; Kawashima, H.; Saji, H.; Fukuyama, H. Quantification of nicotinic acetylcholine receptors in Parkinson's disease with [^{123}I]-5IA SPECT. *J. Neurol. Sci.* **2007**, *256*, 52–60.

(5) Wullner, U.; Gundisch, D.; Herzog, H.; Minnerop, M.; Joe, A.; Warnecke, M.; Jessen, F.; Schutz, C.; Reinhardt, M.; Eschner, W.; Klockgether, T.; Schmaljohann, J. Smoking upregulates alpha4beta2* nicotinic acetylcholine receptors in the human brain. *Neurosci. Lett.* **2008**, *430*, 34–37.

(6) Picard, F.; Bruel, D.; Servent, D.; Saba, W.; Fruchart-Gaillard, C.; Schollhorn-Peyronneau, M. A.; Roumenov, D.; Brodtkorb, E.; Zuberi, S.; Gambardella, A.; Steinborn, B.; Hufnagel, A.; Valette, H.; Bottlaender, M. Alteration of the in vivo nicotinic receptor density in ADNFLE patients: a PET study. *Brain* **2006**, *129*, 2047–2060.

(7) Pichika, R.; Easwaramoorthy, B.; Collins, D.; Christian, B. T.; Shi, B.; Narayanan, T. K.; Potkin, S. G.; Mukherjee, J. Nicotinic alpha4beta2 receptor imaging agents: part II. Synthesis and biological evaluation of 2-[^{18}F]fluoro-3-[2-((*S*)-3-pyrrolinyl)methoxy]pyridine (^{18}F-nifene) in rodents and imaging by PET in nonhuman primate. *Nucl. Med. Biol.* **2006**, *33*, 295–304.

(8) Ding, Y. S.; Kil, K. E.; Lin, K. S.; Ma, W.; Yokota, Y.; Carroll, I. F. A novel nicotinic acetylcholine receptor antagonist radioligand for PET studies. *Bioorg. Med. Chem. Lett.* **2006**, *16*, 1049–1053.

(9) Roger, G.; Saba, W.; Valette, H.; Hinnen, F.; Coulon, C.; Ottaviani, M.; Bottlaender, M.; Dolle, F. Synthesis and radiosynthesis of [^{18}F]FPhEP, a novel alpha(4)beta(2)-selective, epibatidine-based antagonist for PET imaging of nicotinic acetylcholine receptors. *Bioorg. Med. Chem.* **2006**, *14*, 3848–3858.

(10) Gao, Y.; Horti, A. G.; Kuwabara, H.; Ravert, H. T.; Hilton, J.; Holt, D. P.; Kumar, A.; Alexander, M.; Endres, C. J.; Wong, D. F.; Dannals, R. F. Derivatives of (−)-7-Methyl-2-(5-(pyridinyl)pyridin-3-yl)-7-

azabicyclo[2.2.1]heptane are potential ligands for positron emission tomography imaging of extrathalamic nicotinic acetylcholine receptors. *J. Med. Chem.* **2007**, *50*, 3814–3824.
(11) Brown, L. L.; Kulkarni, S.; Pavlova, O. A.; Koren, A. O.; Mukhin, A. G.; Newman, A. H.; Horti, A. G. Synthesis and evaluation of a novel series of 2-chloro-5-((1-methyl-2-(*S*)-pyrrolidinyl)methoxy)-3-(2-(4-pyridinyl)vinyl) pyridine analogues as potential positron emission tomography imaging agents for nicotinic acetylcholine receptors. *J. Med. Chem.* **2002**, *45*, 2841–2849.
(12) Chefer, S. I.; Pavlova, O. A.; Zhang, Y.; Vaupel, D. B.; Kimes, A. S.; Horti, A. G.; Stein, E.; Mukhin, A. G. NIDA522131, a new radioligand for imaging extrathalamic nicotinic acetylcholine receptors: in vitro and in vivo evaluation. *J. Neurochem.* **2008**, *104*, 306–315.
(13) Carroll, F. I.; Ma, W.; Yokota, Y.; Lee, J. R.; Brieaddy, L. E.; Navarro, H. A.; Damaj, M. I.; Martin, B. R. Synthesis, nicotinic acetylcholine receptor binding, and antinociceptive properties of 3′-substituted deschloroepibatidine analogues. Novel nicotinic antagonists. *J. Med. Chem.* **2005**, *48*, 1221–1228.
(14) Zhang, Y.; Pavlova, O. A.; Chefer, S. I.; Hall, A. W.; Kurian, V.; Brown, L. L.; Kimes, A. S.; Mukhin, A. G.; Horti, A. G. 5-substituted derivatives of 6-halogeno-3-((2-(*S*)-azetidinyl)methoxy)pyridine and 6-halogeno-3-((2-(*S*)-pyrrolidinyl)methoxy)pyridine with low picomolar affinity for alpha4beta2 nicotinic acetylcholine receptor and wide range of lipophilicity: potential probes for imaging with positron emission tomography. *J. Med. Chem.* **2004**, *47*, 2453–2465.
(15) Liang, F.; Navarro, H. A.; Abraham, P.; Kotian, P.; Ding, Y. S.; Fowler, J.; Volkow, N.; Kuhar, M. J.; Carroll, F. I. Synthesis and nicotinic acetylcholine receptor binding properties of exo-2-(2′-fluoro-5′-pyridinyl)-7-azabicyclo-[2.2.1]heptane: a new positron emission tomography ligand for nicotinic receptors. *J. Med. Chem.* **1997**, *40*, 2293–2295.
(16) Perry, D. C.; Kellar, K. J. [^{3}H]Epibatidine labels nicotinic receptors in rat brain: an autoradiographic study. *J. Pharmacol. Exp. Ther.* **1995**, *275*, 1030–1034.
(17) Xiao, Y.; Kellar, K. J. The comparative pharmacology and up-regulation of rat neuronal nicotinic receptor subtype binding sites stably expressed in transfected mammalian cells. *J. Pharmacol. Exp. Ther.* **2004**, *310*, 98–107.
(18) Quik, M.; Bordia, T.; O'Leary, K. Nicotinic receptors as CNS targets for Parkinson's disease. *Biochem. Pharmacol.* **2007**, *74*, 1224–1234.
(19) Waterhouse, R. N. Determination of lipophilicity and its use as a predictor of blood−brain barrier penetration of molecular imaging agents. *Mol. Imaging Biol.* **2003**, *5*, 376–389.
(20) Pacheco, M. A.; Pastoor, T. E.; Lukas, R. J.; Wecker, L. Characterization of human alpha4beta2 neuronal nicotinic receptors stably expressed in SH-EP1 cells. *Neurochem. Res.* **2001**, *26*, 683–693.
(21) Xiao, Y.; Fan, H.; Musachio, J. L.; Chellappan, S. K.; Wei, Z. L.; Kozikowski, A. P.; Kellar, K. J. Sazetidine-A, a novel ligand that desensitizes {alpha}4 {beta}2 nicotinic acetylcholine receptors without activating them. *Mol. Pharmacol.* **2006**, 1454–1460.
(22) Lukas, R. J.; Changeux, J. P.; Le Novere, N.; Albuquerque, E. X.; Balfour, D. J.; Berg, D. K.; Bertrand, D.; Chiappinelli, V. A.; Clarke, P. B.; Collins, A. C.; Dani, J. A.; Grady, S. R.; Kellar, K. J.; Lindstrom, J. M.; Marks, M. J.; Quik, M.; Taylor, P. W.; Wonnacott, S. International Union of Pharmacology. XX. Current status of the nomenclature for nicotinic acetylcholine receptors and their subunits. *Pharmacol. Rev.* **1999**, *51*, 397–401.
(23) Laruelle, M.; Slifstein, M.; Huang, Y. Relationships between radiotracer properties and image quality in molecular imaging of the brain with positron emission tomography. *Mol. Imaging Biol.* **2003**, *5*, 363–375.
(24) de Paulis, T. The discovery of epidepride and its analogs as high-affinity radioligands for imaging extrastriatal dopamine D(2) receptors in human brain. *Curr. Pharm. Des.* **2003**, *9*, 673–696.
(25) Zhang, Y.; Horti, A. G. Synthesis of 6-chloro-3-((2-(*S*)-azetidinyl-)methoxy)-5-(2-[^{18}F]fluoropyridin-4-yl)pyridine ([^{18}F]NIDA 522131), a novel potential radioligand for studying extrathalamic nicotinic acetylcholine receptors by PET. *J. Labelled Compd. Radiopharm.* **2004**, *47*, 947–952.
(26) Valette, H.; Bottlaender, M.; Coulon, C.; Ottaviani, M.; Syrota, A. Anesthesia affects the disposition of [^{18}F]fluoro-A-85380: a PET study in monkeys. *Synapse* **2002**, *44*, 58–59.
(27) Van Hemelrijck, J.; Fitch, W.; Mattheussen, M.; Van Aken, H.; Plets, C.; Lauwers, T. Effect of propofol on cerebral circulation and autoregulation in the baboon. *Anesth. Analg.* **1990**, *71*, 49–54.
(28) Hilton, J.; Yokoi, F.; Dannals, R. F.; Ravert, H. T.; Szabo, Z.; Wong, D. F. Column-switching HPLC for the analysis of plasma in PET imaging studies. *Nucl. Med. Biol.* **2000**, *27*, 627–630.
(29) Horti, A. G.; Scheffel, U.; Koren, A. O.; Ravert, H. T.; Mathews, W. B.; Musachio, J. L.; Finley, P. A.; London, E. D.; Dannals, R. F. 2-[^{18}F]fluoro-A-85380, an in vivo tracer for the nicotinic acetylcholine receptors. *Nucl. Med. Biol.* **1998**, *25*, 599–603.
(30) Vaupel, D. B.; Tella, S. R.; Huso, D. L.; Wagner, V. O., 3rd; Mukhin, A. G.; Chefer, S. I.; Horti, A. G.; London, E. D.; Koren, A. O.; Kimes, A. S. Pharmacological and toxicological evaluation of 2-fluoro-3-(2(*S*)-azetidinylmethoxy)pyridine (2-F-A-85380), a ligand for imaging cerebral nicotinic acetylcholine receptors with positron emission tomography. *J. Pharmacol. Exp. Ther.* **2005**, *312*, 355–365.
(31) Scheffel, U.; Horti, A. G.; Koren, A. O.; Ravert, H. T.; Banta, J. P.; Finley, P. A.; London, E. D.; Dannals, R. F. 6-[^{18}F]Fluoro-A-85380: an in vivo tracer for the nicotinic acetylcholine receptor. *Nucl. Med. Biol.* **2000**, *27*, 51–56.
(32) Spande, T. F.; Garraffo, H. M.; Edwards, M. W.; Yeh, H. J. C.; Pannell, L.; Daly, J. W. Epibatidine: a novel (chloropyridyl)azabicycloheptane with potent analgesic activity from an Ecuadoran poison frog. *J. Am. Chem. Soc.* **1992**, *114*, 3475–3478.
(33) Horti, A. G.; Scheffel, U.; Kimes, A. S.; Musachio, J. L.; Ravert, H. T.; Mathews, W. B.; Zhan, Y.; Finley, P. A.; London, E. D.; Dannals, R. F. Synthesis and evaluation of *N*-[^{11}C]methylated analogues of epibatidine as tracers for positron emission tomographic studies of nicotinic acetylcholine receptors. *J. Med. Chem.* **1998**, *41*, 4199–4206.
(34) Brown, L.; Chefer, S.; Pavlova, O.; Vaupel, D. B.; Koren, A. O.; Kimes, A. S.; Horti, A. G.; Mukhin, A. G. Evaluation of 5-(2-(4-pyridinyl)vinyl)-6-chloro-3-(1-methyl-2-(*S*)-pyrrolidinylmethoxy)py ridine and its analogues as PET radioligands for imaging nicotinic acetylcholine receptors. *J. Neurochem.* **2004**, *91*, 600–612.
(35) Kozikowski, A. P.; Chellappan, S. K.; Henderson, D.; Fulton, R.; Giboureau, N.; Xiao, Y.; Wei, Z. L.; Guilloteau, D.; Emond, P.; Dolle, F.; Kellar, K. J.; Kassiou, M. Acetylenic pyridines for use in PET imaging of nicotinic receptors. *ChemMedChem* **2006**, *2*, 54–57.
(36) Spivak, C. E.; Lupica, C. R.; Oz, M. The endocannabinoid anandamide inhibits the function of alpha4beta2 nicotinic acetylcholine receptors. *Mol. Pharmacol.* **2007**, *72*, 1024–1032.
(37) Murase, K.; Ryu, P. D.; Randic, M. Excitatory and inhibitory amino acids and peptide-induced responses in acutely isolated rat spinal dorsal horn neurons. *Neurosci. Lett.* **1989**, *103*, 56–63.
(38) Xiao, Y.; Meyer, E. L.; Thompson, J. M.; Surin, A.; Wroblewski, J.; Kellar, K. J. Rat alpha3/beta4 subtype of neuronal nicotinic acetylcholine receptor stably expressed in a transfected cell line: pharmacology of ligand binding and function. *Mol. Pharmacol.* **1998**, *54*, 322–333.
(39) Black, K. J.; Snyder, A. Z.; Koller, J. M.; Gado, M. H.; Perlmutter, J. S. Template images for nonhuman primate neuroimaging: 1. Baboon. *Neuroimage* **2001**, *14*, 736–743.
(40) Akaike, H. A. new look at statistical model identification. *IEEE Trans. Autom. Control* **1974**, *AU-19*, 716–722.
(41) Logan, J.; Fowler, J. S.; Volkow, N. D.; Wang, G. J.; Ding, Y. S.; Alexoff, D. L. Distribution volume ratios without blood sampling from graphical analysis of PET data. *J. Cereb. Blood Flow Metab.* **1996**, *16*, 834–840.
(42) Ichise, M.; Liow, J. S.; Lu, J. Q.; Takano, A.; Model, K.; Toyama, H.; Suhara, T.; Suzuki, K.; Innis, R. B.; Carson, R. E. Linearized reference tissue parametric imaging methods: application to [^{11}C]DASB positron emission tomography studies of the serotonin transporter in human brain. *J. Cereb. Blood Flow Metab.* **2003**, *23*, 1096–1112.
(43) Chefer, S. I.; Horti, A. G.; Koren, A. O.; Gundisch, D.; Links, J. M.; Kurian, V.; Dannals, R. F.; Mukhin, A. G.; London, E. D. 2-[^{18}F]F-A-85380: a PET radioligand for a4b2 nicotinic acetylcholine receptors. *NeuroReport* **1999**, *10*, 2715–2721.
(44) Valette, H.; Bottlaender, M.; Dolle, F.; Guenther, I.; Fuseau, C.; Coulon, C.; Ottaviani, M.; Crouzel, C. Imaging central nicotinic acetylcholine receptors in baboons with [^{18}F]fluoro-A-85380. *J. Nucl. Med.* **1999**, *40*, 1374–1380.
(45) Gallezot, J. D.; Bottlaender, M.; Gregoire, M. C.; Roumenov, D.; Deverre, J. R.; Coulon, C.; Ottaviani, M.; Dolle, F.; Syrota, A.; Valette, H. In vivo imaging of human cerebral nicotinic acetylcholine receptors with 2-^{18}F-fluoro-A-85380 and PET. *J. Nucl. Med.* **2005**, *46*, 240–247.
(46) Chefer, S. I.; London, E. D.; Koren, A. O.; Pavlova, O. A.; Kurian, V.; Kimes, A. S.; Horti, A. G.; Mukhin, A. G. Graphical analysis of 2-[^{18}F]FA binding to nicotinic acetylcholine receptors in rhesus monkey brain. *Synapse* **2003**, *48*, 25–34.

JM800323D